UNCLASSIFIED

AD NUMBER

AD362544

LIMITATION CHANGES

TO:

Approved for public release; distribution is unlimited.

FROM:

Distribution authorized to U.S. Gov't. agencies only; Test and Evaluation; APR 1960. Other requests shall be referred to Air Force Space System Division, Attn: SSZD, Los Angeles, CA.

AUTHORITY

NRO ltr dtd 21 Nov 2012

THIS PAGE IS UNCLASSIFIED

UNCLASSIFIED

AD NUMBER
AD362544
CLASSIFICATION CHANGES
TO: **UNCLASSIFIED**
FROM: **CONFIDENTIAL**
AUTHORITY
30 APR 1972, dodd 5200.10

THIS PAGE IS UNCLASSIFIED

UNCLASSIFIED

AD NUMBER
AD362544
CLASSIFICATION CHANGES
TO: **CONFIDENTIAL**
FROM: **SECRET**
AUTHORITY
30 APR 1963, dodd 5200.10

THIS PAGE IS UNCLASSIFIED

SECURITY MARKING

The classified or limited status of this report applies to each page, unless otherwise marked.
Separate page printouts MUST be marked accordingly.

"This document contains information affecting the National Defense of the United States within the meaning of the Espionage Laws, Title 18, U. S. C., Section 793 and 794. Its transmission or the revelation of its contents in any manner to an unauthorized person is prohibited by law."

DOWNGRADED AT 3 YEAR INTERVALS:
DECLASSIFIED AFTER 12 YEARS
DOD DIR 5200.10

"ONE HALF ORIGINAL SIZE"

attachment A

AIR FORCE
TECHNICAL DATA CENTER
TECHNICAL LIBRARY
Document No. 61-04-7232
Copy No. 1/1

[redacted]

CONFIDENTIAL

DOCUMENT NO. R60SD340

TECHNICAL INFORMATION SERIES

NO. R60SD340

TITLE

Thermal Restudy of the Discoverer Mark 2 (Bio-Med) Vehicle

AUTHOR

J. Segletes
H. P. Strickberger

This folder is the property of the General Electric Company, and must not be retained except by special permission, or used directly or indirectly in any way detrimental to the interest of the Company.

FN-612 (12-68)

This document may be released to other government agencies upon request. No release will be made to non-government companies or individuals without specific approval of the Program Director at Hq Space System Div., Los Angeles 45, Calif., Attn: SSZD.

ASTIA
RECEIVED
MAY 7 1963
TIPDR

MISSILE AND SPACE VEHICLE DEPARTMENT

GENERAL ELECTRIC

DOWNGRADED AT 3 YEAR INTERVALS
DECLASSIFIED AFTER 12 YEARS.
DOD DIR 5200.10

[redacted]

CONFIDENTIAL

61-04-7232
2037-44-2

[redacted]

CONFIDENTIAL

SECURITY NOTICE

NOTICE: This document contains information affecting the national defense of the United States within the meaning of the Espionage Laws, Title 18 U.S.C., Sections 793 and 794. Its transmission or the revelation of its contents in any manner to an unauthorized person is prohibited by law.

This document may be released to other government agencies upon request. No release will be made to non-government companies or individuals without specific approval of the Program Director at Hq Space System Div., Los Angeles 45, Calif., Attn: SSZD.

CONFIDENTIAL

[redacted]

[redacted]

CONFIDENTIAL

FOR USE OF G.E. EMPLOYEES ONLY

(5) GENERAL ELECTRIC Co., Philadelphia, Pa.
MISSILE AND SPACE VEHICLE DEPARTMENT Div.

TECHNICAL INFORMATION SERIES

Title Page This document contains 72 numbered pages.
Copy number 27 of 60 copies.

AUTHOR	SUBJECT CLASSIFICATION	No.
(11) by J. Segletes and H. P. Strickberger	(14) Rept. Thermodynamic Analysis	R60SD340
		DATE (11) April 1960, (12) 72 p.

TITLE

(6) Thermal Restudy of the Discoverer Mark 2 (Bio-Med) Vehicle (U)

(15) Contract AF 04(647)-97

ABSTRACT

A restudy of the thermal performance of the Discoverer Mark 2 vehicle has been made. Exposure to the predicted extreme thermal environments (hottest, coldest) is studied. Fixes are recommended and/or limitations are presented if exposure to the extreme environments indicate possible problems.

G.E. CLASS	REPRODUCIBLE COPY FILED AT	No. PAGES
IV	Documents Library Missile and Space Vehicle Dept. Philadelphia, Pa.	72
GOV. CLASS. Secret		

CONCLUSIONS

This document may be released to other government agencies upon request. No release will be made to non-government contractors or individuals without specific approval of the Program Director at Missile Systems Div., Los Angeles 45, Calif., Attn: SSLD.

By cutting out this rectangle and folding on the center line, the above information can be fitted into a standard card file.

For list of contents—drawings, photos, etc. and for distribution see next page (FN-610-2).

INFORMATION PREPARED FOR Contract AF 04(647)-97

PREPARED BY John A Segletes, J. Segletes, Aerophysics Engrg. Harold P. Strickberger, H. P. Strickberger, Aerophysics Engrg.

COUNTERSIGNED J. D. Stewart, J. D. Stewart, Manager - Aerophysics Engineering Operation

DIVISIONS Defense Electronics LOCATION 3198 Chestnut Street, Philadelphia 4, Penna.

DOWNGRADED AT 3 YEAR INTERVALS;
DECLASSIFIED AFTER 12 YEARS.
DOD DIR 5200.10

[redacted]

CONFIDENTIAL

1

2037-14-2

Previous page was blank, therefore not filmed.

CONTENTS

ILLUSTRATIONS

[redacted]

CONFIDENTIAL

ILLUSTRATIONS (CONT'D)

CONFIDENTIAL CONFIDENTIAL

[redacted]

ILLUSTRATIONS (CONT'D)

[redacted]

CONFIDENTIAL

TABLES

CONFIDENTIAL

[redacted]

1. INTRODUCTION

A restudy of the thermal performance of the Discoverer Mark 2 vehicle has been made; documentation is presented herein. Temperature and char histories of the existing design, when exposed to the extreme thermal environments (hottest, coldest), are determined. Fixes are recommended and/or limitations are presented if exposure to the extreme environments indicates possible problems.

A portion of the study (LMSD adapter and adjacent MSVD components) will be issued as a supplement. Figure 1 gives the configuration of the Discoverer Mark 2 vehicle and the adjoining LMSD adapter section.

2. INPUTS USED IN STUDY

2.1 POWERED FLIGHT

2.1.1 Initial Temperatures. Initial life cell temperatures at the time of launch were assumed to be between 60° F and 80° F in the analysis although the temperature specification is 65° F to 85° F. This approach was used in the analysis because the maintenance of an average initial temperature between 60° F and 80° F appeared realistic since:

a. In a similar program, takeoff temperatures between 60° F and 80° F were assured. See reference 1.

b. In a Mark 1 flight, Discoverer II, where the minimum specification temperature was to be 65°F, the temperature was below 60°F. With ground air circulation provisions included in the design, the launch temperature can be controlled to the valued desired.

2.1.2 Trajectories. Powered flight trajectories of the hottest and coldest cases are shown in figures 2 and 3 respectively. The powered flight trajectory of the hottest case, a trajectory which would inject a Discoverer vehicle into a nominal 98 statute mile perigee orbit, was originally obtained from digital printout sheets supplied by LMSD. The Discoverer II powered flight trajectory, reduced from data appearing in reference 2, is assumed to be representative of the coldest case. The perigee altitude of the Discoverer II orbit was 158 statute miles, 8 miles higher than the predicted Mark 2 maximum orbit altitude.

2.1.3 Internal Heat Generation. Internal heat generation during powered flight is presented in column A of table 1.

2.1.4 Transition Reynolds Number (turbulent to laminar). Based on flight test data appearing in reference 2, a transition Reynolds number expressed as a function of wetted length (Re_s), of 350,000 is used.

2.1.5 Pressure Distribution. The coefficient of pressure ratio (C_p/C_p max.), used for the powered flight portion of this study is shown in figure 4.

TABLE I. INTERNAL HEAT GENERATION

Internal Heat Generation During all Phases (Btu/hr)												
Component	A Powered Flight		B Orbit		C Re-entry		D Parachute Descent		E Air Pickup		F Water Flotation	
	Max.	Min.	Max.	Min.	Max.	Min.	Max.	Min.	Max.	Min.	Max.	Min.
1. Conditioner	64	41	64	41	64	41	64	41	64	41	64	41
*2. Life Cell Subject	21	14	21	14	21	14	21	14	21	14	21	14
Life Cell Heater	0	0	0	34	0	0	0	0	0	0	0	0
Life Cell Components	45	45	45	45	51.5	51.5	51.5	51.5	51.5	51.5	29.5	29.5
3. Water Evaporator (see note 2)	0	0	64.0	0	0	0	0	0	0	0	0	0
4. Beacon Battery Heater	0	0	0	17	0	0	0	0	0	0	0	0
5. Thermal Battery	0	0	0	0	283.0 BTU Total	283.0 BTU Total	0	0	0	0	0	0

Note:

1. The maximum and minimum values in this table allow for the possible variation in heat dissipation of the animal.
2. Value given of the water evaporator is the heat removal rate during the hot orbit from the life cell and conditioner.

* 25% - Body Heat, 75% - Heat from the reaction of carbon-dioxide with chemicals in the conditioner.

SECRET
CONFIDENTIAL
SECRET
CONFIDENTIAL

This curve represents modified Newtonian distribution over the nose faired into the Kopal value downstream.

2.1.6 Thrust Cone Temperature. Thrust cone temperature histories for calculating internal component temperatures forward of station 27 are shown in figure 5. These curves, obtained from a previous study, are actually for an explosive bolt which is mounted near the thrust cone.

2.2 ORBITAL FLIGHT

2.2.1 Trajectory Definition. The perigee altitude - eccentricity envelope which defines the bounds of the Discoverer flights (reference 3) is shown in figure 6. The 3σ capabilities of the Agena booster (reference 4) are also shown in figure 6.

Perigee location is between 15° N and 45° N latitude (reference 4).

2.2.2 Adapter Equilibrium Temperatures. Equilibrium temperatures of the adapter section for the hottest and coldest cases are calculated from data appearing in reference 5. These temperatures are 540° R for the hottest case and 485° R for the coldest case. For the analysis, it is conservatively assumed that these temperatures are also the equilibrium temperatures of the thrust cone.

2.2.3 Internal Heat Generation. Internal heat generation during orbital flight is presented in column B of table 1.

During orbital flight of the hottest case, sixty-four BTU's per hour are removed from the life cell by the water evaporator.

2.2.4 Heat Fluxes. Table II presents a breakdown of the orbital heat flux parameters:

TABLE II. ORBITAL HEAT FLUX PARAMETERS

Heat Source	Nominal Value	Tolerance
Solar Radiation $\frac{BTU}{Ft^2\text{-}HR}$	460 (Jan. 2) 435 (Jul. 5)	$\pm$ 3%
Albedo Factor	.36	+ 0.16 (predominantly cloudy skies) - 0.16 (predominantly clear skies)
Earth's Radiation $\frac{BTU}{Ft^2\text{-}HR}$	70.2	+ 15% (predominantly clear skies) - 15% (predominantly cloudy skies)
Free molecule heating	Negligible (Re-entry vehicle at aft end during orbital flight)	

2.3 RE-ENTRY FLIGHT

2.3.1 Initial Trajectory Conditions. A broadening of the orbital trajectory envelope at the initiation of this study also broadened the envelope of possible re-entry trajectories. As a result, reference 6 estimated the initial re-entry conditions used in this study and then started an extensive parametric study to accurately determine the new range of re-entry conditions that could occur. Results of the parametric study show that: (1) 1.79° and 3.87° are the limiting path angles at 325,000 ft. alt. (2) the originally estimated initial velocities are sufficiently accurate, (3) for an orbit probability of 85% (see figure 6), the limiting path angles are 2.18° and 3.58°.

Originally estimated initial conditions which are used to calculate trajectories are given in table III.

TABLE III. ESTIMATED INITIAL CONDITIONS FOR CALCULATING TRAJECTORIES

Flight Parameter	Hottest Case	Coldest Case
Path angle-deg. (down from local horizontal)	1.5	4.61
velocity-ft/sec. (relative to air)	26,350	26,390
weight-lb.	203 (heaviest)	188 (lightest)
altitude-ft.	325,000	325,000

2.3.2 Internal Heat Generation. Internal Heat Generation during re-entry is presented in column C of table I.

2.3.3 Aerodynamic Characteristics. The $C_p/C_{p\,max.}$ distribution used to calculate aerodynamic heat fluxes is shown in figure 7. This distribution was calculated by a digital program which uses techniques described in reference 7.)

The coefficient of drag-mach number relationship used to calculate re-entry trajectories is shown in figure 8.

The angle of attack convergence envelope used to calculate the effect of pitching motion on the aerodynamic heat fluxes is shown in figure 9.

The base pressure ratios $\left(\frac{P_b}{P_\infty}, \frac{P_b}{P_s}\right)$ as a function of mach number are shown in figure 10.

2.4 PARACHUTE DESCENT AND AIR PICK-UP/WATER FLOTATION

2.4.1 Parachute Descent Phase

2.4.1.1 Trajectory. The parachute trajectory used in this study is shown in figure 11.

2.4.1.2 Atmospheric Model. Atmospheric properties are based on the MSVD tropical atmosphere. A comparison between the MSVD tropical and the ARDC 1956 model atmospheres is shown in figure 12.

2.4.1.3 Internal Heat Generation. Internal heat generation during parachute descent is shown in column D of table I.

2.4.2 Air Pickup Phase. The assumptions of the air pickup phase are as follows:

a. The altitude at air pickup is between 0-14,000 ft. (If the pickup occurs at a high altitude, presumably the airplane will descend to an altitude of approximately 2,500 feet where the ambient air temperature is higher.

b. The time required to pull the capsule into the airplane is 20 minutes.

c. The airplane speed will be a constant 194 ft/sec.

2.4.3 Water Flotation. The water temperature is assumed to be 535°R.

3. DISCUSSION OF METHOD

3.1 POWERED FLIGHT

3.1.1 Shield Performance. Aerodynamic heat transfer coefficients and recovery enthalpies are calculated by a digital computer program for 30 body locations along one meridian of the Discoverer Mark 2 re-entry vehicle. The atmosphere is represented by the ARDC 1956 model. The ARDC 1959 model atmosphere officially replaced the 1956 model soon after the initiation of this study. However, we think that the new model would have a negligible effect on the results of the powered flight portion of this study. When Re_s is less than 350,000, aerodynamic heat transfer equations based on Lester Lees's classical solution of the hypersonic heating problem (laminar boundary layer) are used. When Re_s is greater than 350,000, aerodynamic heat transfer equations based on the turbulent flat plate law are used.

Heat transfer coefficients and recovery enthalpies at three body locations (stagnation point, beginning of skirt, end of skirt) combined with other pertinent data are used as input to a digital conduction-ablation program. A closed loop method uses the input and the self-generated surface temperature to calculate the instantaneous heat flux. Temperature histories of approximately 40 points within the shield and the front face recession history are simultaneously calculated based on the self-generated instantaneous heat flux.

Shield temperature calculations are based on an adiabatic back face.

Calculated hot gas and solar radiations are small when compared with aerodynamic heating; consequently they are neglected.

3.1.2 Temperature of Internal Components. To facilitate computations, the internal problem is divided into two sections. The first section considers only those components forward of station 27. The second section considers only those components to the rear of the aft cover which is approximately at station 27.

3.1.2.1 Forward of Station 27. Temperature histories of the shield's back face and thrust cone during powered flight are used as input to a digital conduction-radiation program which calculates the temperatures of internal components forward of station 27.

The thermal capacitance of each major component is determined. Major components are then "linked" by thermal radiating and conducting paths. The physical thermal system is then expressed as an analogous electrical network of resistances and capacitances. The electrical network is then greatly simplified by replacing portions of the network with simple equivalent networks. By this technique the complete system which thermally represents the

interior of the Mark 2 vehicle is simplified enough to be programmed on the IBM 704 digital computer.

3.2 ORBITAL FLIGHT

3.2.1 Temperature of Internal Components . As in powered flight, the internal problem is divided into two sections to facilitate computations. It is assumed that all components inside of and attached to the life cell are at the same temperature as the life cell air temperature unless otherwise noted. This becomes apparent when consideration is given to the good conduction paths between components and the life cell housing. In addition, the convection effect on the inside of the life cell tends to stabilize the temperatures. Tests performed on the unit also bear out this effect.

3.2.1.1 Forward of Station 27. Representation of the thermal system of internal components forward of station 27 during orbital flight is fundamentally the same as that described in section 3.1.2.1. During orbital flight, however, a thermal boundary condition is imposed at the outside surface of the shield in lieu of the inside. Hence, it is necessary to insert additional network (representing the shield) between the driving outer boundary and the internal components.

Instead of imposing a heat flux at the shield's outer surface, its equivalent in the form of a space sink temperature is used. The space sink temperature is obtained by first determining the mean effective heat flux (with respect to both time and body location) and then determining the re-radiating (space sink) temperature of the mean effective flux. An infinite capacitance node having the space sink temperature is then coupled by a radiation link to the shield of the thermal system.

Past computer runs and simulation tests (reference 8), which used a programmed cyclic heat flux to the shield's surface, indicated that temperature oscillations will be damped out before reaching the capsule. The tests also indicated that the circumferential temperature profile on the capsule will not be significant. Hence, the space sink approximation is considered valid.

From the time of orbit injection until equilibrium is reached, the thrust cone temperature is taken as the extrapolation of the thrust cone temperatures used during powered flight.

3.2.1.2 Experimental Verification of the Discoverer Mark 2 Analytical Model. Thermal-altitude tests were conducted at LMSD's Bemco facility to verify the Discoverer Mark 2 design for orbital flight. Good agreement between predicted and measured temperatures was obtained. A comparison of analytical results with values which would be expected if test data were used is shown in some of the figures in this report. See reference 8 also.

3.3 RE-ENTRY

3.3.1 Heat Flux to Shield. Zero angle of attack convective heat fluxes based on point mass trajectories and a nonablating configuration are calculated by a digital trajectory-flux program for 30 body locations along one meridian of the shield's outer surface. The atmosphere is represented by the ARDC 1956 model. The recently published ARDC 1959 model atmosphere would have a negligible effect on the results covering the re-entry portion of this study.

When Re_s is less than 100,000, heat fluxes based on Lester Lees's classical solution of the hypersonic heating problem (laminar boundary layer) are used. When Re_s is greater than 100,000, equations based on the turbulent flat plate law are used. Flight test data of the WS 107A and WS 315A programs indicate that transition on a nonablating shape occurs when $Re_s \cong 400,000$. Our supressed value of transition ($Re_s = 100,000$) accounts for the destabilizing effects of mass addition and surface roughness.

Hot gas radiation heat fluxes are calculated by the trajectory-flux program. A technique which relates the flux to the thickness, temperature, and density of the gas cap is used.

The pitching motion correction factor is obtained by calculating the laminar convective heat flux at a body location for several angles of attack. Care is taken to select angles of attack that permit the heat flux to be determined by standard techniques. For instance, when the angle of attack is 90°, the flow around the skirt region of the Mark 2 re-entry vehicle approximates the flow around a cylinder. For a given radius, the convective heat flux to the stagnation line of a cylinder is 0.707 times the heat flux to the stagnation point of a sphere (reference 9). A plot of heat flux vs. angle of attack is made at peak heating for each body location of interest. Mean effective heat fluxes between several angles of attack of equal magnitude and opposite sign are calculated for each body location of interest. The mean effective heat fluxes are divided by zero angle of attack heat fluxes which are also calculated at peak heating. The ratio thus obtained is the factor which is used to correct the computer calculated heat fluxes for pitching motion.

Pitching motion correction factors in dimensionless form $\left(\frac{\dot{q}_{\alpha \neq 0}}{\dot{q}_{\alpha = 0}}\right)$ are shown in figure 13 as a function of angle of attack for the three body locations studied (stagnation point, beginning of skirt, end of skirt).

Use of the above method assumes the following:

a. Harmonic pitching motion

b. Pitching in one plane only

c. No spin

d. All laminar heating

e. The shield response to a cyclic heat flux can be approximated by an average of the cyclic heat flux.

Although the angle of attack correction factor is developed specifically for the convective heat flux, the correction factor is assumed to also apply to the hot gas radiative flux since $\dot{q}_{HGR} \cong 1\%$ of $\dot{q}$ conv. The error introduced by this approximation is insignificant.

3.3.2 Response of Shield. Temperature and char responses of the basic shield at three locations (stagnation point, beginning of skirt, end of skirt) are calculated by a digital conduction-char ablation program. Primary inputs consist of gross heat fluxes to the shield's external surface (extrapolated to alt = 400,000 ft) and thermal properties which are experimentally determined. The first set of computer runs calculates the the temperature responses of both the basic phenolic-glass shield and the epoxy-polysulfide coating until the coating is removed. The second set of computer runs calculates the temperature and char responses of the basic phenolic-glass shield from the time of coating removal until the gross re-entry heat flux becomes negative (alt $\cong$ 100,000 ft). Shield temperature histories are extrapolated during the cooling phase of re-entry.

An adiabatic shield back face is assumed.

3.3.3 Afterbody Environment and Temperature Response. The heat flux to the aft cover and the simultaneous temperature responses of the aft cover, back-up insulation, and nylon parachute are calculated by a digital flux-conduction program. Detached flow heat flux equations, based on flight test data from the WS 107A and WS 315A programs, are used. Transition from laminar to turbulent flow on the aft cover is assumed to occur when Re_s at the end of the skirt reaches 100,000.

Afterbody heat fluxes assume a zero angle of attack. At altitudes above 310,000 feet however, the precessional motion of the vehicle exposes the aft cover to a severer thermal environment than that predicted for a zero angle of attack. It is estimated that the effect of the increased heating on the predicted parachute temperatures would be negligible because:

1. The duration of the increased heating is relatively small (approximately 40 seconds for the hottest case).

2. The magnitude of the net heat flux is small due to:

   a. High altitude.

   b. Concave profile of the afterbody.

   c. Increased amount of reradiated heat.

3.3.4 Temperature of Internal Components. Internal component temperatures are calculated by a digital conduction-radiation program which uses as input the heat fluxes at the aft cover's outer surface and temperature histories at the shield's char line. As already described in section 3.1.2.1 for powered flight heating, the thermal system which represents the internal components is reduced to a relatively simple analogous electrical network of resistances and capacitances.

3.4 PARACHUTE DESCENT AND AIR PICKUP/WATER FLOTATION

3.4.1 External Environment After separation of the capsule from the shield, the convective heat flux to the surface is obtained from correlated data of spheres and cones.

Solar, albedo, and earth's radiations are neglected.

3.4.2 Internal Temperatures. Internal temperatures are calculated by a digital conduction-radiation-convection program which, as in the other phases of flight, simulates conditions by an analogous electrical network. Here, however, the network covers only the capsule. Boundary conditions are heat transfer coefficients and ambient temperatures imposed at the outer surface of the capsule.

3.5 WATER FLOTATION. If air pickup is unsuccessful, water flotation is assumed.

Internal temperatures are calculated by a digital conduction-radiation-convection program. The capsule temperature is assumed to be the same as the water temperature (535°R).

4. TOLERANCES ON TEMPERATURE PREDICTIONS

As can be inferred from section 3 (DISCUSSION OF METHOD), the study is broken into distinct work blocks which are joined in time and space by the interrelated boundary conditions. In some cases the break-up is to facilitate computations. In other cases the break-up is necessitated by the complexity of the problem (e.g. three dimensional heating with char formation).

The work blocks used in this study are as follows:

a. External environment and thermal shield forward of station 27 during powered flight.

b. Internal components forward of station 27 during powered flight.

c. External environment of the LMSD adapter during powered flight.

d. Internal components aft of station 27 and the LMSD adapter section during powered flight.

e. External environment, thermal shield, and internal components forward of station 27 during oribital flight.

f. External environment, LMSD adapter, and internal components aft of station 27 during orbital flight.

g. External environment and thermal shield forward of station 27 during re-entry flight.

h. Wake region environment and afterbody during re-entry flight.

i. Internal components during re-entry flight.

j. External environment, capsule, and internal components during parachute descent and air pickup.

k. External environment, capsule, and internal components during parachute descent and air pickup/water flotation.

The predicted temperatures in each of these work blocks are for nominal values of thermal properties, thicknesses, etc. Realistically, however, tolerances do exist on all of the nominal inputs. Furthermore, the techniques used to generate temperatures introduced additional tolerances. As a consequence, a tolerance on predicted temperatures also exists.

Table IV shows the recommended tolerances to be applied to the predicted temperatures.

TABLE IV. TOLERANCES FOR PREDICTED TEMPERATURES

FLIGHT PHASE	TEMPERATURE TOLERANCE	WORK BLOCK NUMBER
1. Powered Flight		
A. Shield	±0.20 ($T-T_{initial}$)	a
B. Internal Components	±0.20 ($T-T_{initial}$)	b, d
C. External environment of LMSD adapter	N.A.	c
2. Orbital Flight		
A. Shield	±0.10 ($T_{component}-T_{space\ sink}$)	e
B. LMSD Adapter	±0.10 ($T_{component}-T_{space\ sink}$)	f
C. Internal Comp.	±0.10 ($T_{component}-T_{space\ sink}$)	e, f
3. Re-entry Flight		
A. Shield	±0.20 ($T-T_{initial}$)	g
B. Afterbody	±0.20 ($T-T_{initial}$)	h
C. Internal Comp.	±0.20 ($T-T_{initial}$)	i
4. Parachute Descent and Air Pickup/water flotation		
A. Internal Components	±0.1 ($T-T_{initial}$)	j
B. External Environment	N.A.	k

5. RESULTS

5.1 POWERED FLIGHT

5.1.1 Analogous Electrical Model. The simplified electrical network representing the conduction interaction between the internal components during powered flight is shown in figure 14.

5.1.2 Heat Fluxes to External Surface. Convective heat fluxes during powered flight are shown in figures 15 and 16 for the hottest and coldest cases at the stagnation point, the beginning of the skirt, and the end of skirt.

5.1.3 Reynolds Number. Reynolds numbers (Re_s) during powered flight are shown in figures 17 and 18 for the hottest and coldest cases.

5.1.4 Temperature Histories. Shield temperature and ablation histories of the hottest case are presented in figures 19 through 21 for the stagnation point, beginning of skirt, and end of skirt. Histories of the coldest case for the same body locations are shown in figures 22 thru 24. Temperature histories of internal components for the hottest and coldest cases are presented in figures 25 through 28.

5.2 ORBITAL FLIGHT

5.2.1 Analogous Electrical Model and Space Sink Temperature. The simplified electrical network representing the conduction interaction between the internal component during orbital flight is shown in figure 29.

Table V presents the space sink temperature used during orbital flight:

TABLE V. SPACE SINK TEMPERATURE DURING ORBITAL FLIGHT

Item	Hot Case	Cold Case
Re-entry Vehicle	522°R (62 °F)	476°R (16°F)
LMSD Adapter	540°R (80°F)	485°R (25°F)

5.2.2 Temperature Histories. Temperature histories of internal components are presented in figures 30 through 32 for the hottest case. (Beacon battery and life cell heaters are not operating).

Temperature histories of internal components for the coldest case are presented in figures 33 and 34. (Life cell and beacon battery heaters are operating continuously.)

5.3 RE-ENTRY

5.3.1 Analogous Electrical Model . The simplified electrical network representing the conduction interaction between the internal components during re-entry flight is shown in figure 35.

5.3.2 Trajectories Point mass trajectories based on a nonablating body are presented in figures 36 and 37 for the hottest and coldest cases.

5.3.3 Heat Fluxes to External Surface . Re-entry heat fluxes of the hottest and coldest cases for three body locations are shown in figures 38 and 39. Wake heat fluxes for both cases are presented in figure 40.

5.3.4 Reynolds Number Reynolds numbers (Re_s) are shown in figures 41 and 42.

5.3.5 Temperature Histories. Shield temperature and charring histories of the hottest case are presented in figures 43 through 45 for the stagnation point, beginning of skirt, and end of skirt respectively. Histories of the coldest case for the same body locations are shown in figures 46 through 48.

Temperature histories of internal components are shown in figures 49 through 58.

5.4 PARACHUTE DESCENT AND AIR PICKUP/WATER FLOTATION

5.4.1 Analogous Electrical Model The simplified electrical network representing the conduction interaction between the internal components during parachute descent and air pickup is shown in figure 59.

5.4.2 Heat Transfer Coefficients. The heat transfer coefficients used during parachute descent and air pickup are shown in figures 60 and 61, respectively.

5.4.3 Temperature Histories.

5.4.3.1 Parachute Descent . Temperature histories of internal components for the hottest and coldest environments during parachute descent are given in figures 62 through 65.

5.4.3.2 Air Pickup . Temperature histories during air pickup are shown in figure 66 for the coldest case. Air pickup for the hottest case does not present any thermal problems.

5.4.3.3 Water Flotation. The simplified electrical network representing the conduction interaction between the internal components during water flotation is shown in figure 67.

Water flotation tests have indicated that at equilibrium the life cell temperature is 85°F when the water temperature is 75°F.

In figure 68 the temperature histories of internal components for the coldest case are shown after water impact. Since life cell temperatures during parachute descent drop below the specification limit of 65°F, the effects of water flotation were studied to determined the total length of time that life cell temperatures would be below the specification limit of 65°F.

5.5 CRITICAL COMPONENTS. Certain components which have relatively stringent temperature limitations have been given special attention. Table VI presents the predicted temperatures of critical components.

Note that the predicted maximum magnesium ring temperature exceeds the maximum allowable temperature. A special parametric study is made to determine the maximum ring temperature for the revised minimum path angle (1.79°) and the 85% orbit probability minimum path angle (2.18°). An initial re-entry temperature of 520°R is assumed. Magnesium ring temperatures at parachute ejection as a function of path angle are shown in figure 69.

TABLE VI. PREDICTED TEMPERATURE RANGE (°F) OF CRITICAL COMPONENTS

Component	FLIGHT PHASE															Comments
	Powered Flight			Orbital Flight			Re-entry Flight			Parachute Descent			Water Flotation			
	Max.	Minimum		Max.	Minimum		Max.	Minimum		Max.	Minimum		Max.	Minimum		
	A	A		A	A	D	A	A	D	A	A	D	A	A	D	
Sensor Battery	82	65		95	66	50	88	66	50	88	55	40	85	55	40	
Recorder Battery	82	65		95	66	50	88	66	50	88	55	40	85	55	40	
O_2 Fan Battery	82	65		95	66	50	88	66	50	88	55	40	85	55	40	
Camera Light Battery	82	65		95	66	50	88	66	50	88	55	40	85	55	40	
Viability Amplifier Battery	82	65		95	66	50	88	66	50	88	55	40	85	55	40	
Camera Battery	82	65		95	66	50	88	66	50	88	55	40	85	55	40	
Thermal Battery	82	65		95	66	50	550	475								Before Activation 0-165 Allowable At Activation 1000 Max. Allowable
*Antenna Assy.	82	65					520									572 Max. Allowable
*Wire Cutters							165									**165 Max. Allowable
*Beacon Light Assy							125									**20-165 Allowable
*Beacon/Battery Assy	82	65		97	64	50	88	66	50							**40-165 Allowable
*Magnesium Ring							565 (minimum path angle studied, $T_{initial} = 520^{\circ}R$)									450 Max. Allowable

Note:

1. Column Identification:
   A - Primate Alive
   D - Primate Deceased
2. All heaters are off during prelaunch period.
3. Temperature tolerances are included.
4. Temperatures given in table are based on test data where applicable.

* Only the highest temperature for the entire flight is shown.

** These allowable limits are used in qualifying tests. It does not necessarily mean that the component will not perform satisfactorily beyond these limits. Where the qualifying temperature is exceeded by 5°F or less, it is assumed that the component will perform satisfactorily.

SECRET
CONFIDENTIAL
SECRET
CONFIDENTIAL

CONFIDENTIAL

TABLE VII. DEVIATION FROM LIFE CELL TEMPERATURE SPECIFICATIONS

Flight Phase	Time Above $85^{o}F$	Max. Temp. Reached	Referenced Figure	Time Below $65^{o}R$	Minimum Temp. Reached	Referenced Figure
Powered Flight	--	Specification Not Exceeded		--	--	--
Orbital Flight						
$T_{initial} = 80^{o}F$	16 hrs	$95^{o}F$	30	0	--	--
$T_{initial} = 70^{o}F$	14 hrs	$88.5^{o}F$	70	0	--	--
Re-entry and	20 min.	88	51	0	--	--
Parachute Descent			62	25 min.	55	65
Water Flotation	0	--	--	15 min.	55	69

CONFIDENTIAL

6. CONCLUSIONS

6.1 Reference to Table VII indicates that the life cell temperature specification of $75^{o}F \pm 10^{o}F$ can be exceeded at either limit if all of the conditions which can cause a temperature extreme occur at the same time. For example, the highest temperatures could occur if the firing was as late as 3:00 P. M., the powered flight trajectory was the hottest extreme, the overall thermal resistance was the highest, etc. The probability of all extreme conditions occurring at the same time is small but nevertheless possible.

For the hottest orbit with an initial life cell temperature of $80^{o}F$, the maximum specification temperature of the life cell in orbit is exceeded for 16 hours. Figure 70 indicates that lowering the initial temperature of the life cell to $70^{o}F$ results in a maximum temperature of $89^{o}F$ and a violation of the $85^{o}F$ maximum temperature limit for 14 hours. It is apparent that an initial life cell temperature of $65^{o}F$ at launch would result in a maximum temperature of $85^{o}F$ in orbit and hence satisfy the life cell temperature specification.

During the re-entry, parachute descent and water flotation phases, specification temperatures are exceeded for relatively short times (table VII). It should be noted that the ocean water temperature of $75^{o}F$ was used in this report and in field tests. During the summer months the water temperature could reach $83^{o}F$. For this condition, if the capsule is not quickly recovered (within 2 hours), the life cell temperatures could exceed the $85^{o}F$ specification.

To overcome the problems associated with the violation of the temperature specification the following alternatives are considered feasible.

a. For Orbit

1. Require that the initial temperature of the life cell at launch be $65^{o}F$.

2. Consider raising the maximum specification temperature.

3. A combination of a-1 and a-2 as given above.

b. For Re-entry and Parachute Descent for Hot Orbit

1. Change in specification to allow a temperature in excess of $85^{o}F$ for 20 minutes.

2. Additional cooling capacity to keep the life cell temperature below $81^{o}F$ at orbit ejection. (Cooling requirement would be 73 Btu/hr.)

c. For Re-entry, Parachute Descent and Water Flotation for Cold Orbit

1. Change in specification to allow a temperature below 65°F for 40 minutes.

2. Addition of heaters and batteries in life cell to maintain temperature of life cell above 65°F during parachute descent.

3. Addition of heaters to life cell to maintain temperature of life cell at 75°F at orbit ejection. (An additional 10 watts would be required.)

It should also be realized that the Thermal-Altitude Test on Use 72 resulted in an overall thermal resistance of $.325 \pm .06 \frac{^{\circ}F\text{-hr.}}{Btu}$.

The large tolerance on this value is primarily the result of the failure of test instrumentation to function properly. Since the temperature of the life cell during re-entry and parachute descent is dependent on the life cell temperature at orbit ejection, a reduction of the tolerance on the overall thermal resistance would result in a lower predicted life cell temperature for the hottest orbit and a higher predicted life cell temperature for the coldest orbit. For example, if the nominal value of .325 is used for the overall thermal resistance, the life cell temperatures at orbit ejection would be 81°F and 75°F for the hot and cold cases respectively. The temperature specification would then not be exceeded during re-entry or parachute descent.

Temperature predictions indicate that the violation of the temperature specification under the worst possible conditions and assumptions is not excessive. Consideration, however, should be given to testing the vehicle at the extreme conditions expected during powered flight, re-entry and parachute descent.

As shown in figure 69, the temperature of the magnesium ring during parachute ejection is less than the maximum allowable temperature for all path angles greater than 2.15 degrees. A major redesign would be necessary to guarantee the magnesium ring for the entire range of initial re-entry path angles predicted.

With the exception of the life cell and the magnesium ring, all MSVD components are within specification.

REFERENCES:

1. Holser, A., LMSD, Private Communication

2. LMSD, "Use 92 Flight Data" LMSD 434371/62-61 Dated 6/18/59, Secret

3. Hart, J., LMSD, Private Communication

4. Ousley, J., LMSD

5. LMSD Outline of Use 38A Thermal - altitude test program

6. Maynard, L., Flight Mechanics Engineering, MSVD

7. Gravalos, F., Edelfent, I., Emmons, H., "The Supersonic Flow about a Blunt Body of Revolution for Gases at Chemical Equilibrium," TIS R58SD245 Dated 6/16/59

8. Use 38A - Thermal Altitude Test Report #60SD901 Dated 1/13/60

9. Lees, D., "Laminar Heat Transfer over Blunt-nosed Bodies at Hypersonic Flight Speeds."

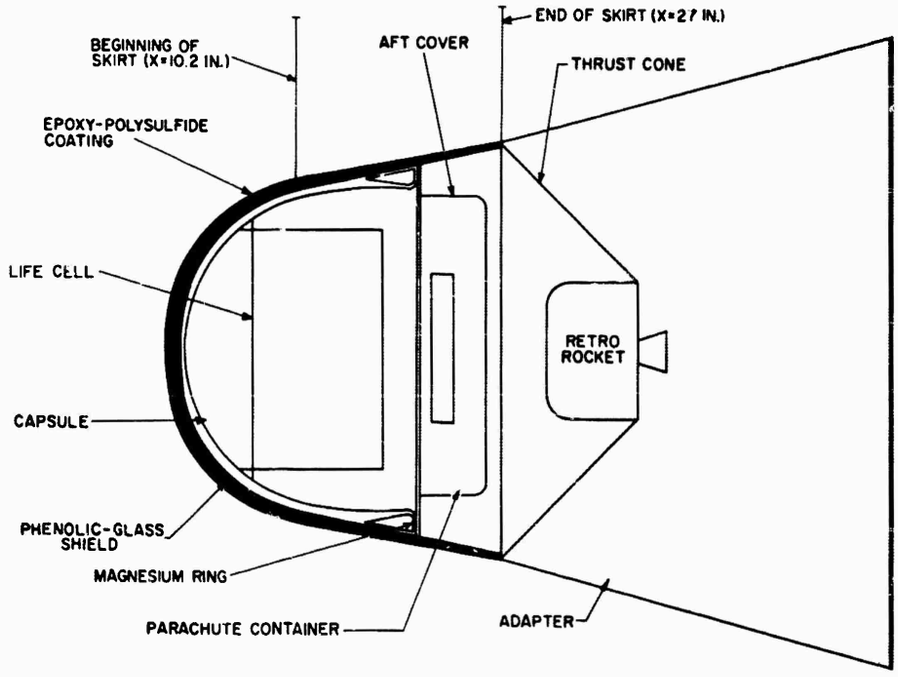

Figure 1. Discoverer Mark 2 Vehicle and Adapter Section

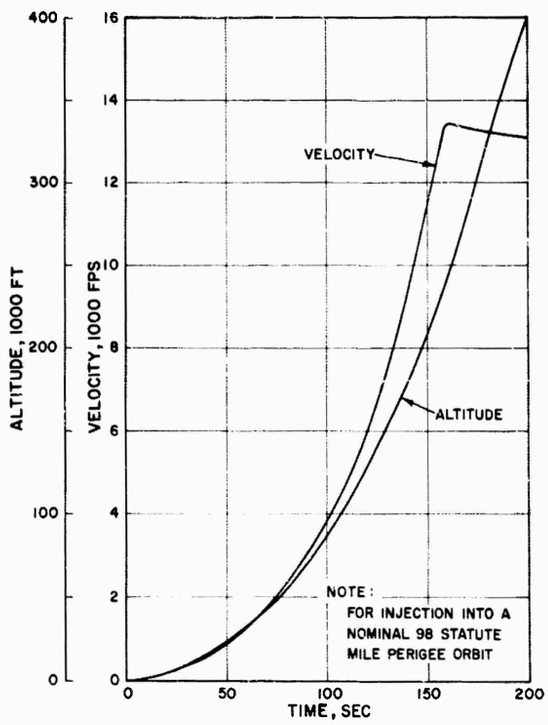

Figure 2. Trajectory During Powered Flight, Hottest Case

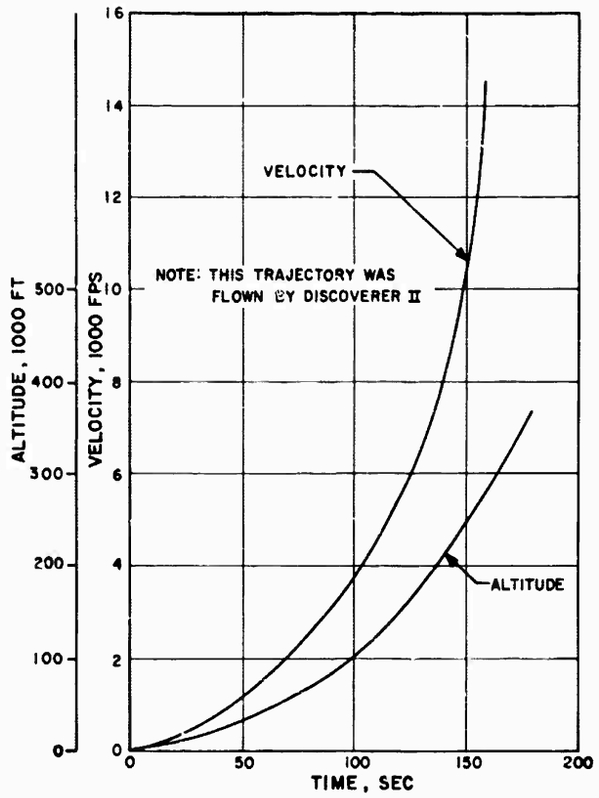

Figure 3. Trajectory During Powered Flight, Coldest Case

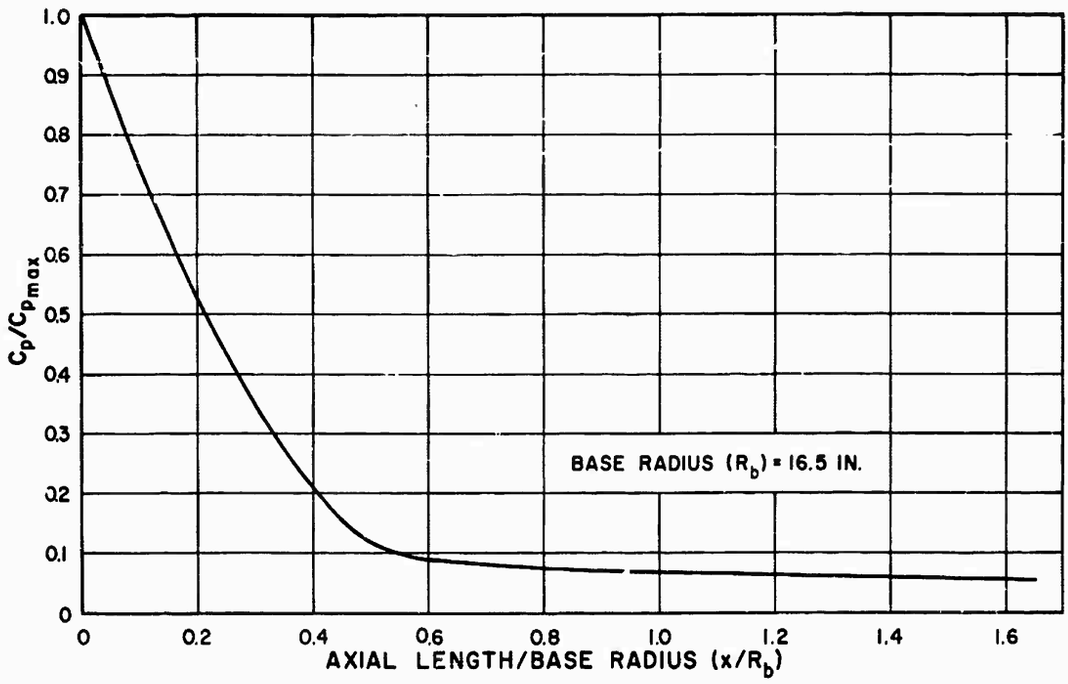

Figure 4. Coefficient of Pressure Distribution During Powered Flight

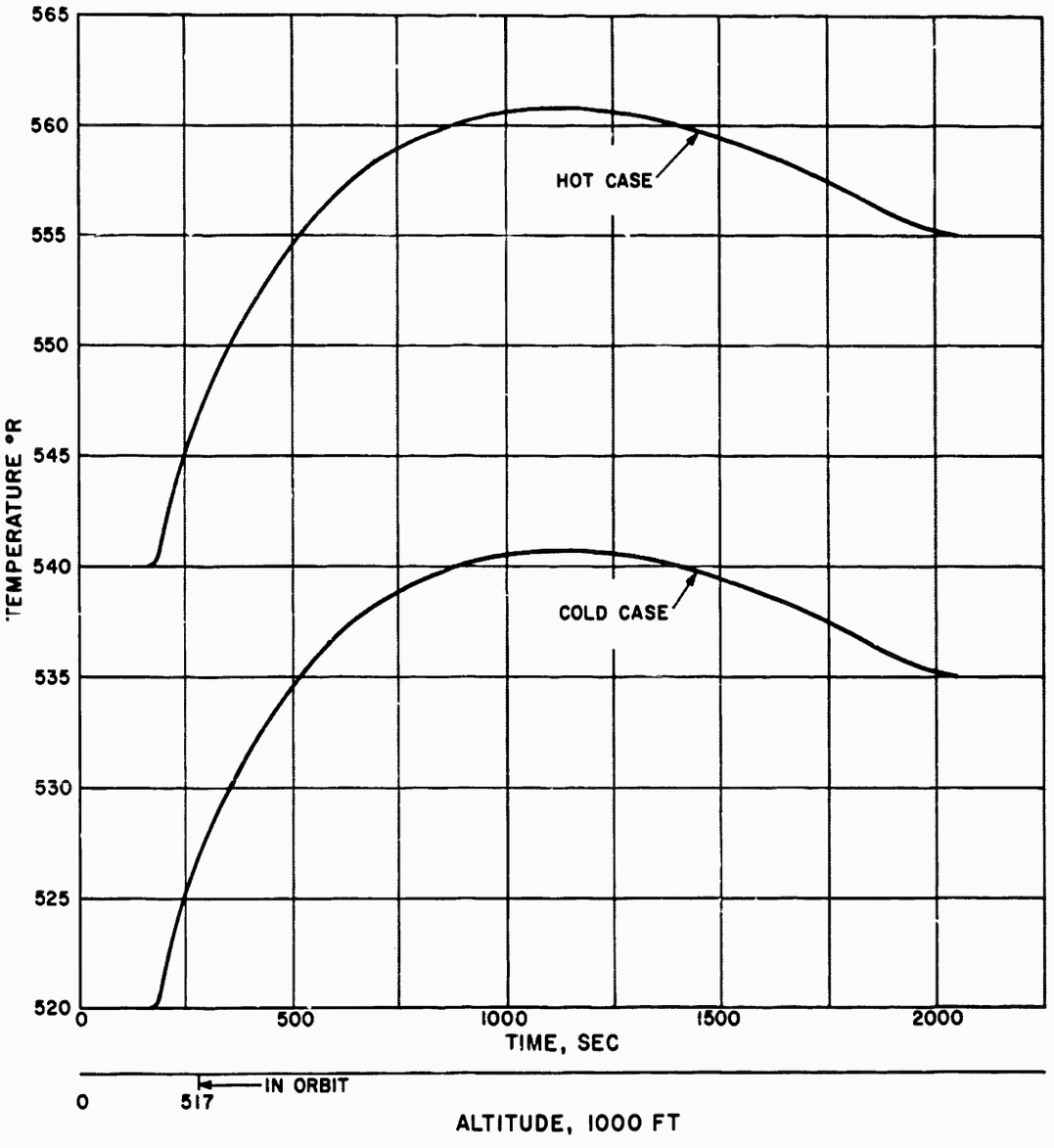

Figure 5. Temperature Histories of Thrust Cone

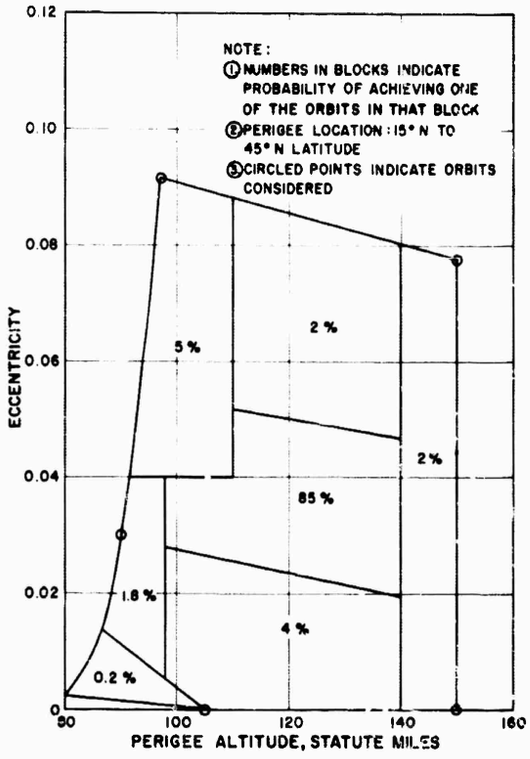

Figure 6. Bounds of Discoverer Flights - Eccentricity vs. Perigree Altitude

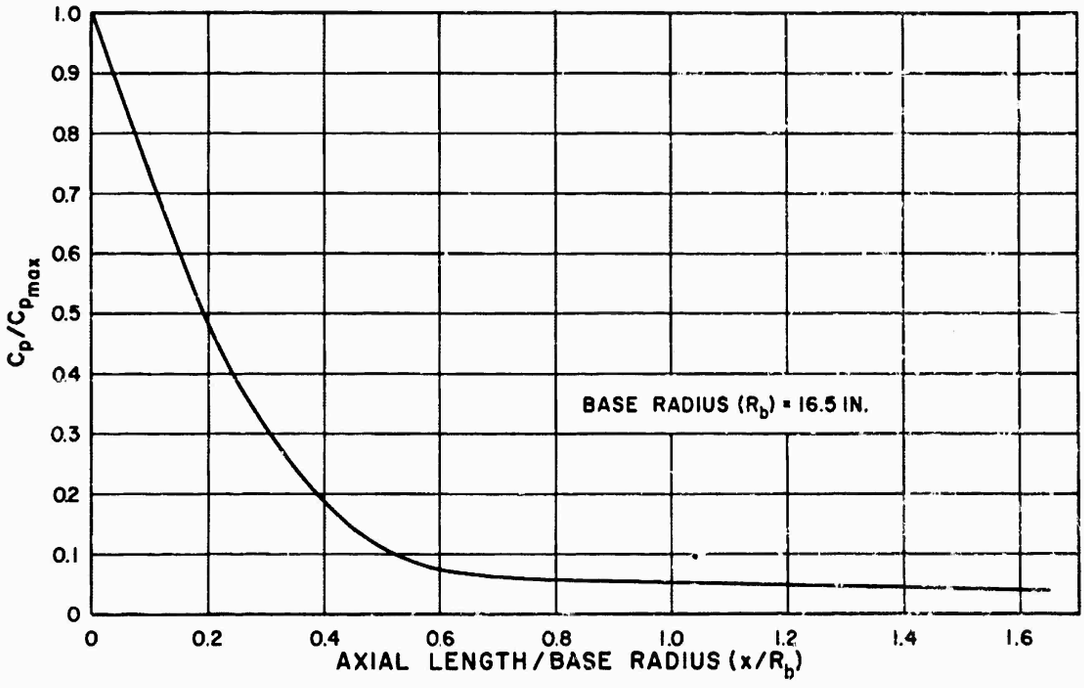

Figure 7. Coefficient of Pressure Distribution During Re-entry

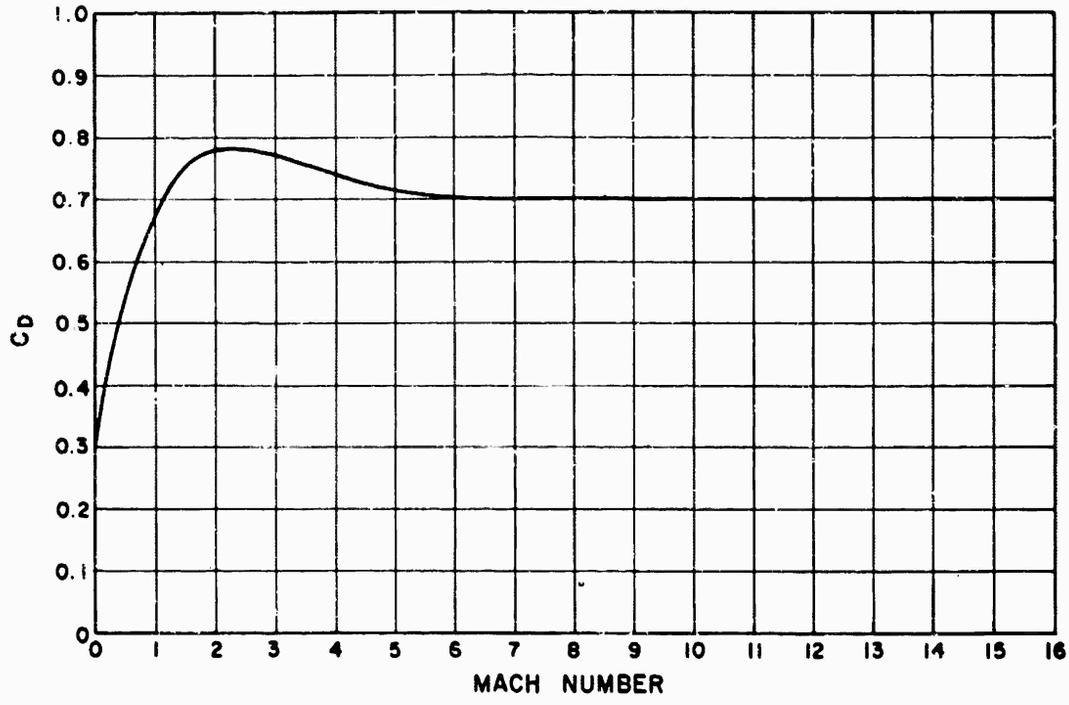

Figure 8. Coefficient of Drag vs. Mach Number During Re-entry

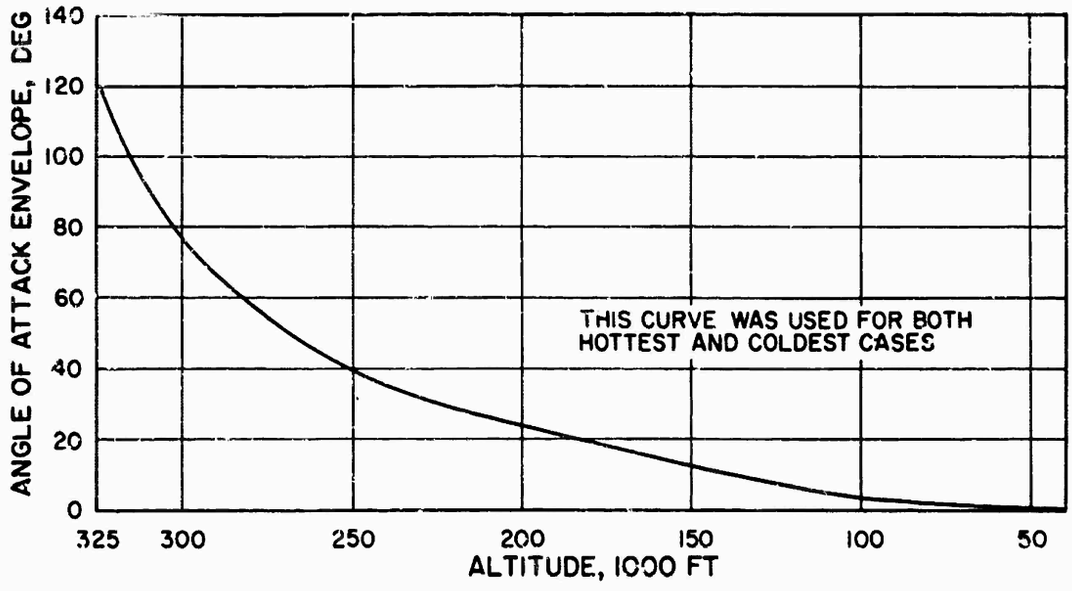

Figure 9. Envelope of Angle of Attack Convergence During Re-entry

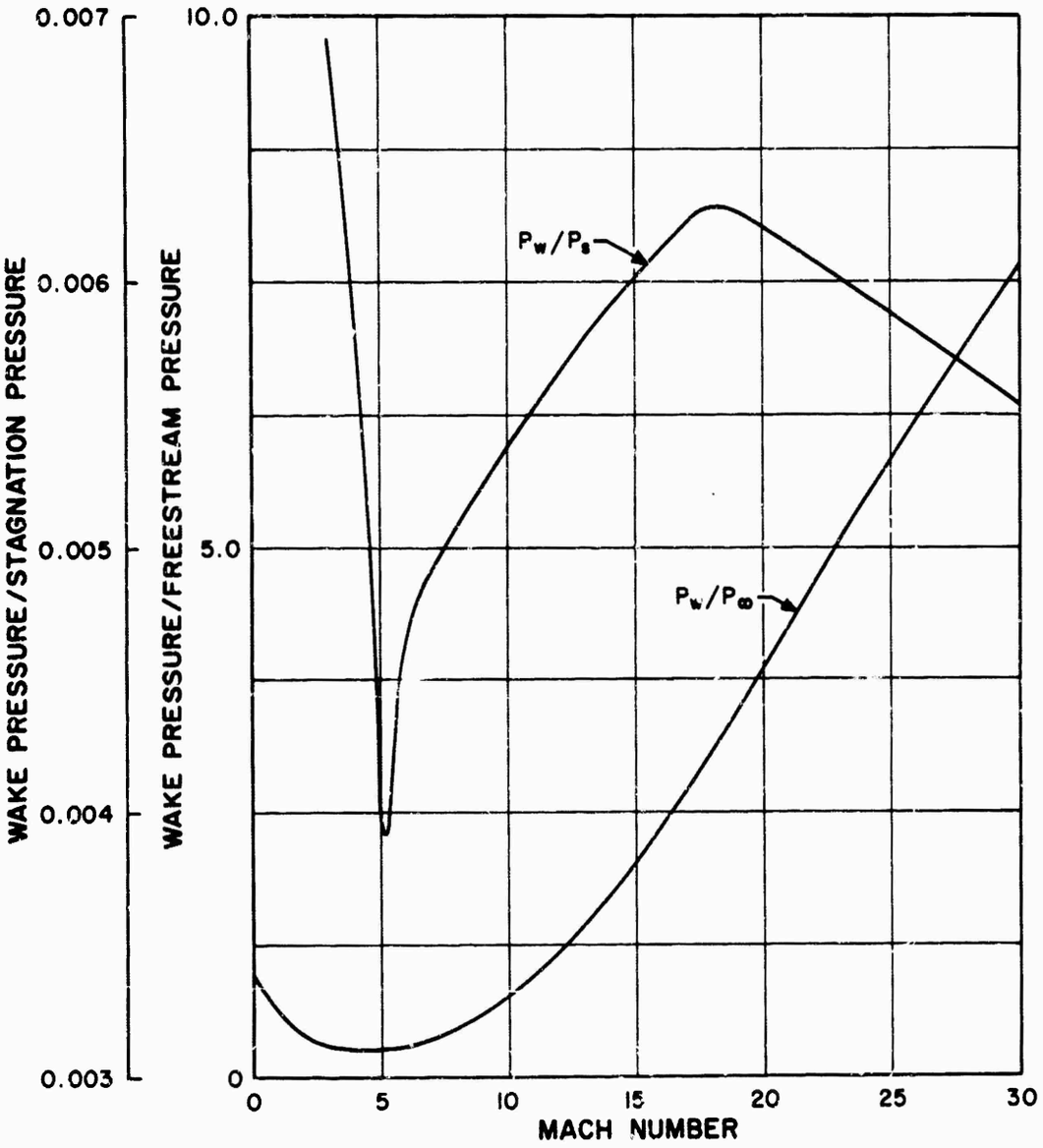

Figure 10. Wake Pressure Ratios vs. Mach Number

CONFIDENTIAL

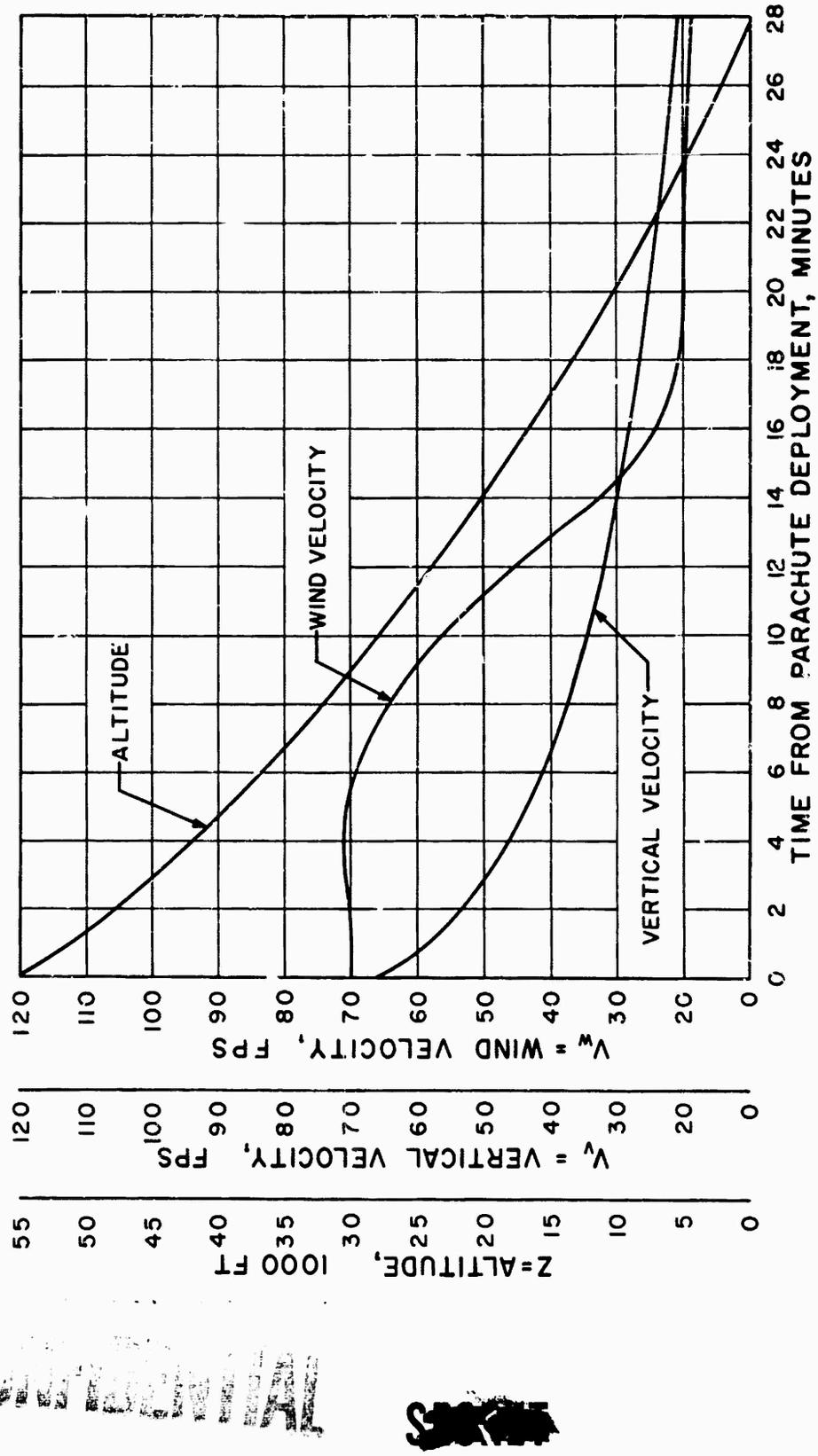

Figure 11. Parachute Trajectory

CONFIDENTIAL

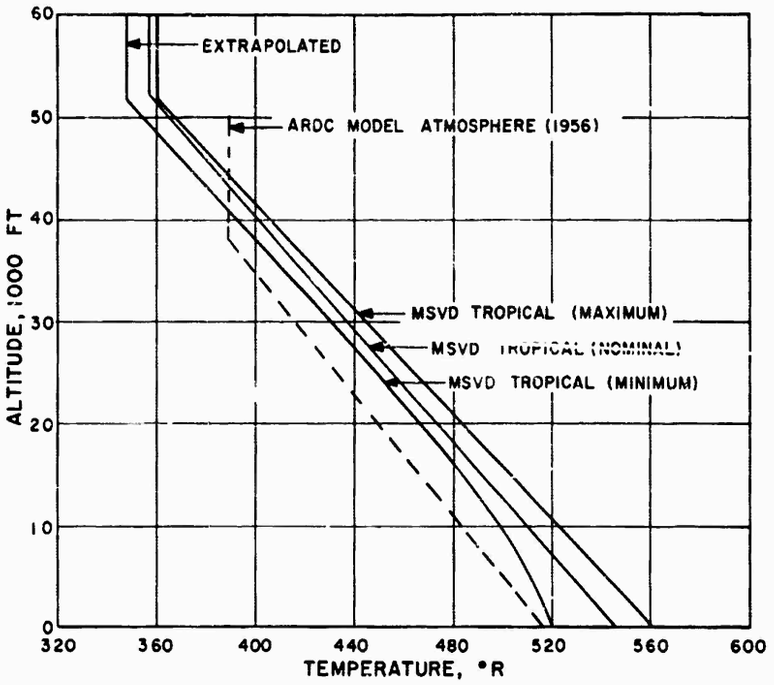

Figure 12. Comparison of MSVD Tropical Atmosphere and 1956 ARDC Model Atmosphere

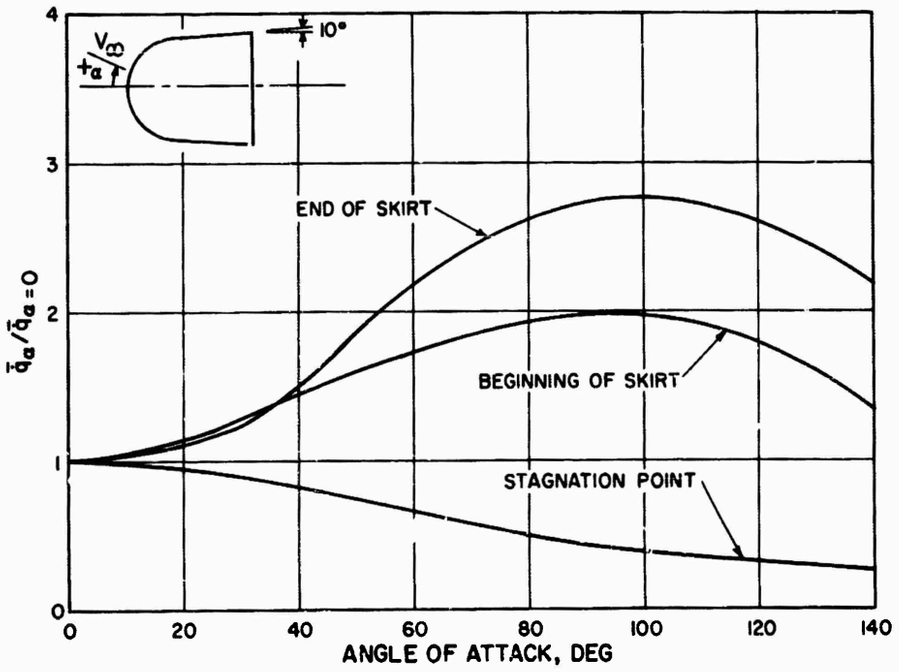

Figure 13. Pitching Motion Correction Factors

CONFIDENTIAL

NOTE: ① CONVECTION IS ASSUMED TO BE NEGLIGIBLE
② NOT ALL RADIATIVE RESISTANCES ARE SHOWN
③ VALUES WITHIN ⬭ ARE HEAT CAPACITIES OF COMPONENTS IN BTU/°F
④ RESISTANCE VALUES ARE IN HR-° F/BTU

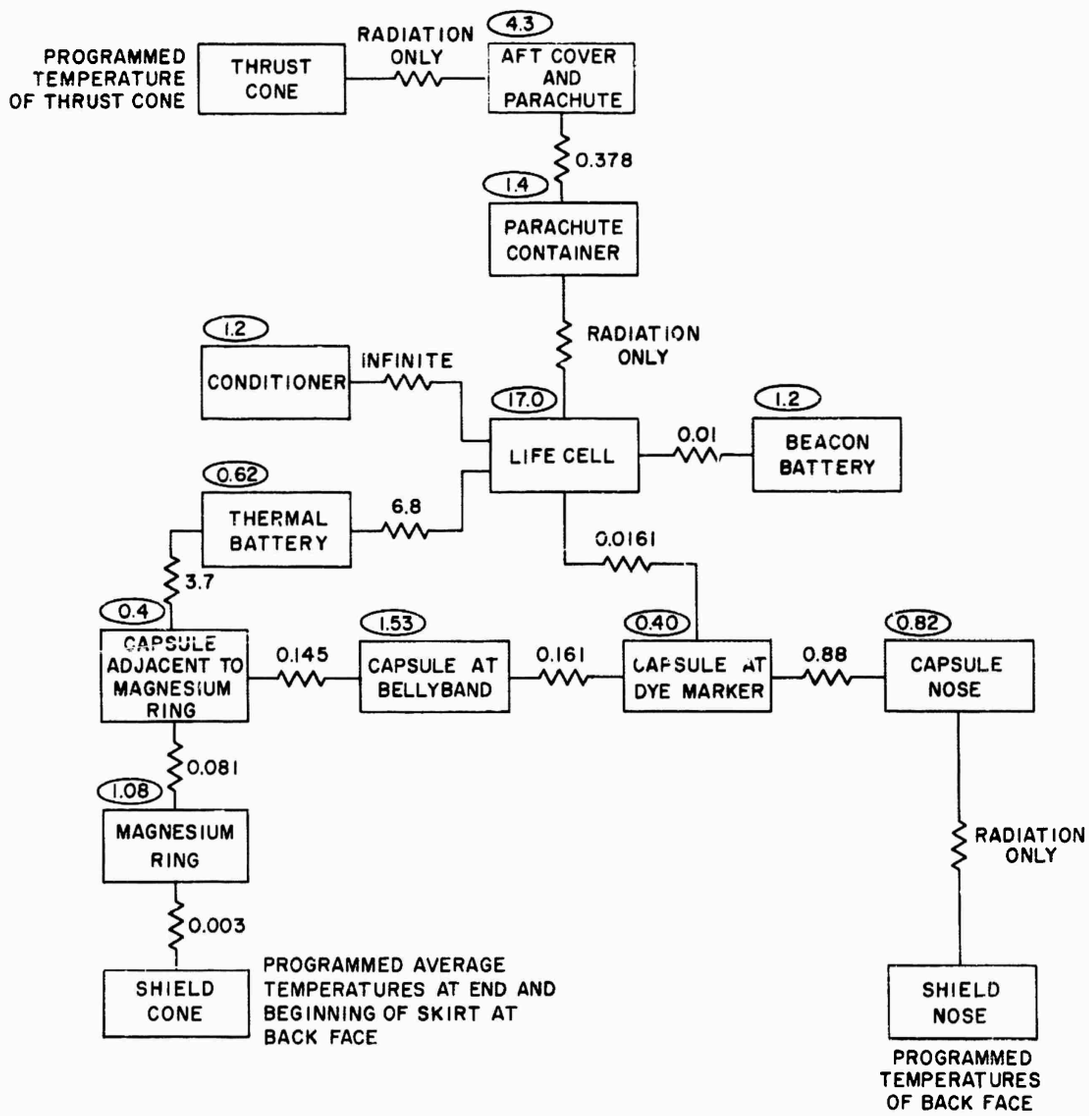

Figure 14. Simplified Electrical Circuit Analogous to Thermal Conduction Between Internal Components During Powered Flight

CONFIDENTIAL

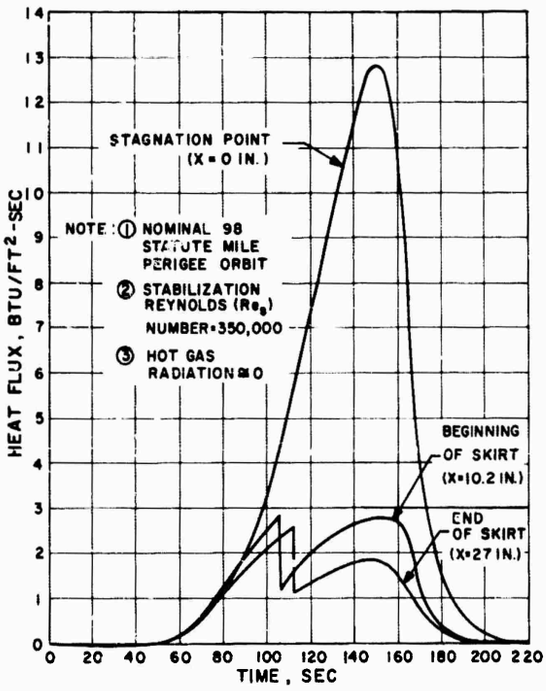

Figure 15. Convective Heat Fluxes During Powered Flight, Hottest Case

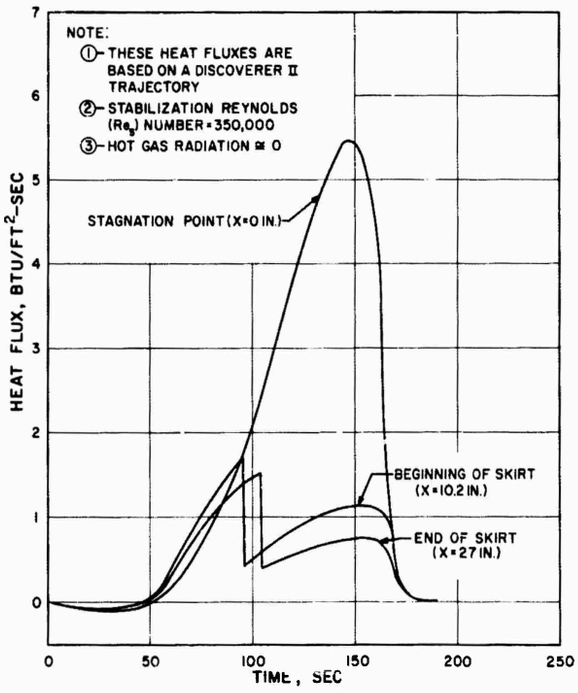

Figure 16. Convective Heat Fluxes During Powered Flight, Coldest Case

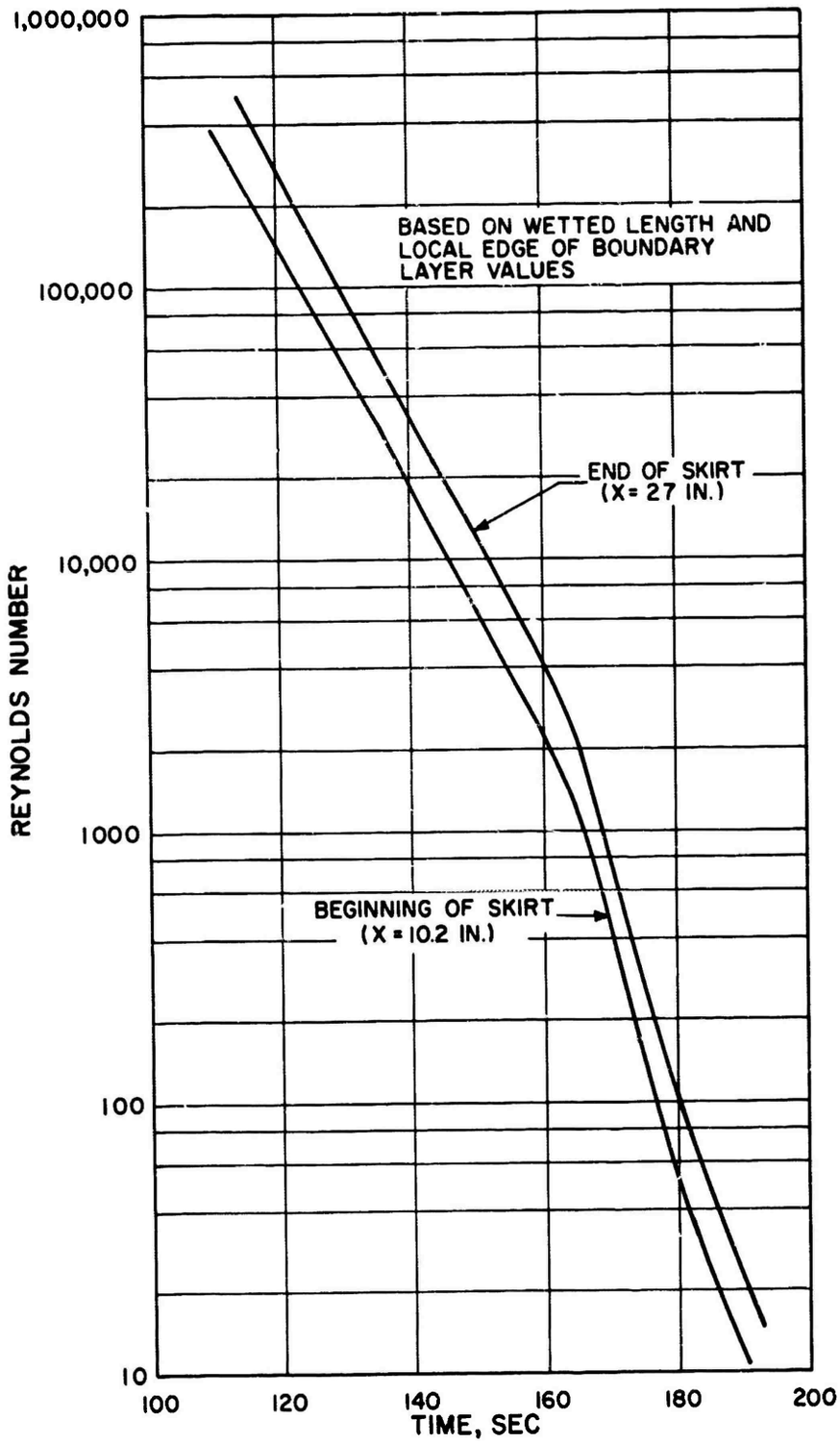

Figure 17. Reynolds Number During Powered Flight, Hottest Case

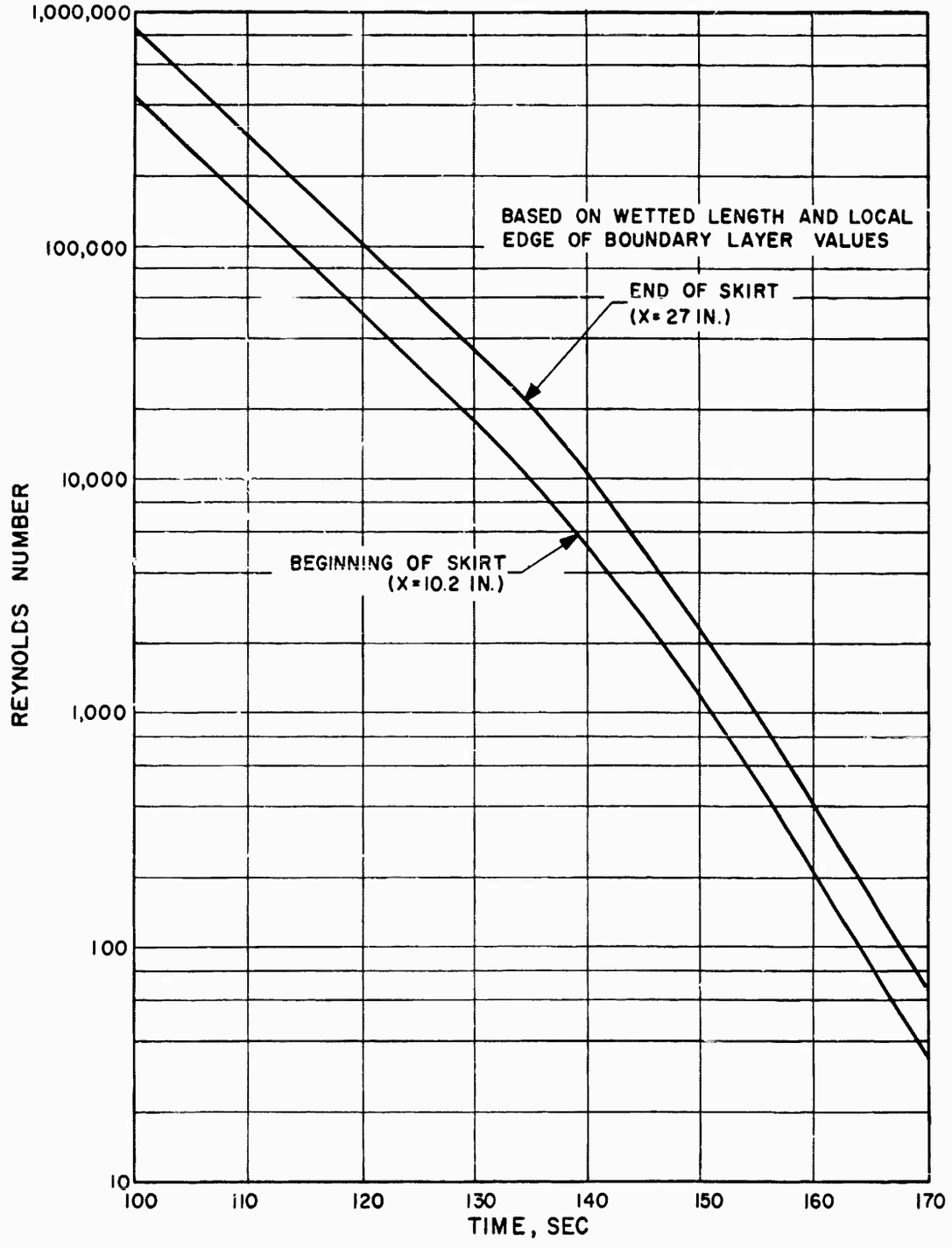

Figure 18. Reynolds Number During Powered Flight, Coldest Case

CONFIDENTIAL

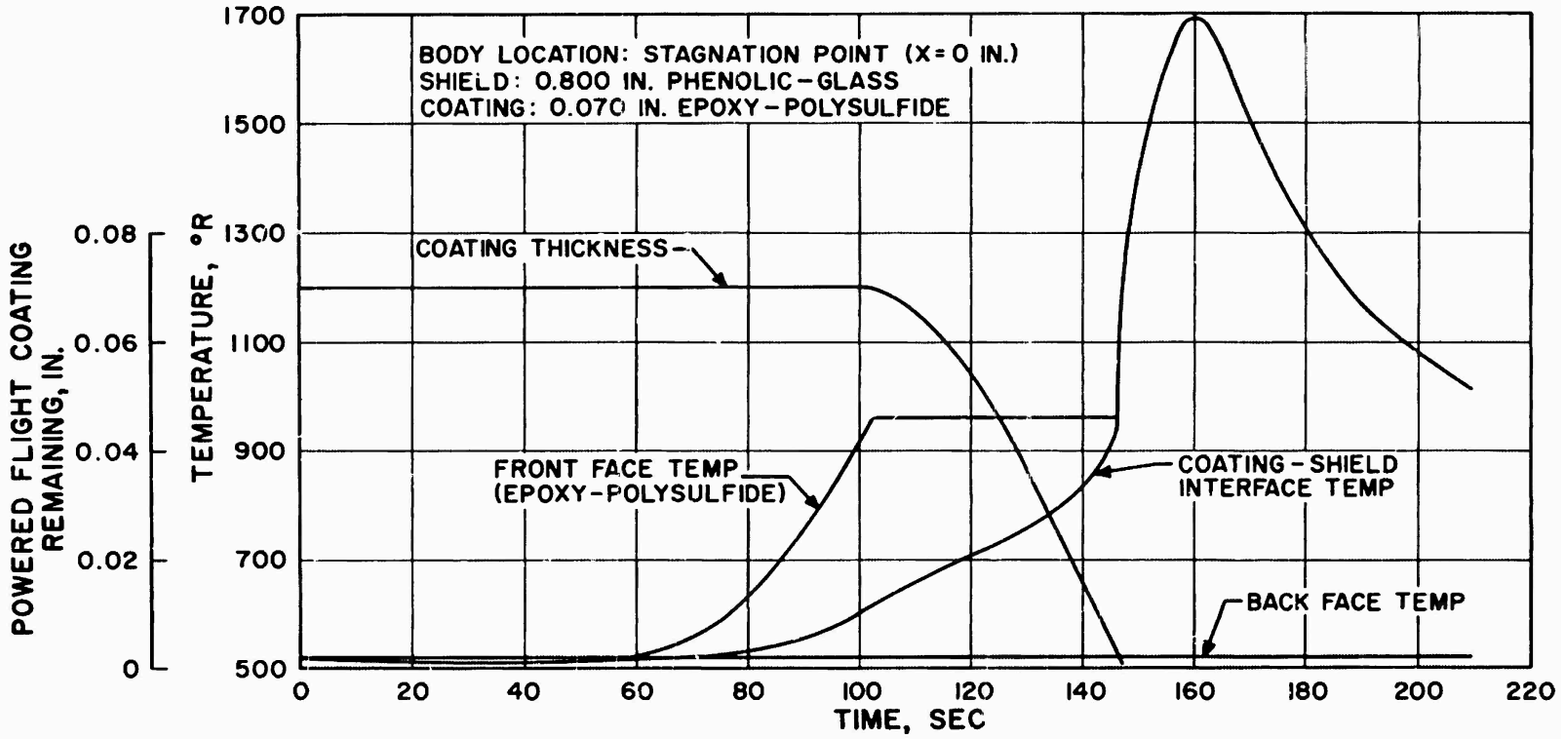

Figure 19. Shield Temperature and Ablation at Stagnation Point During Powered Flight, Hottest Case

CONFIDENTIAL

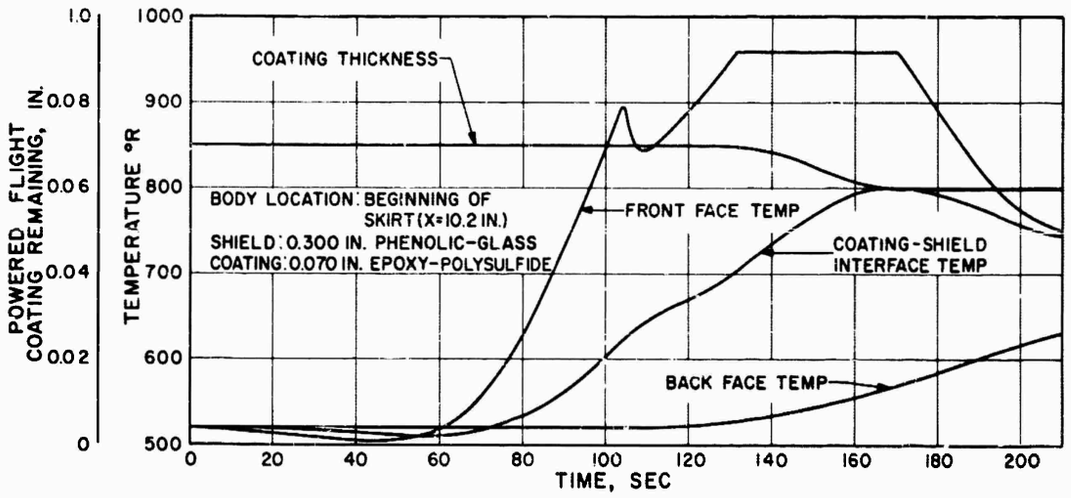

Figure 20. Shield Temperature and Ablation at Beginning of Skirt During Powered Flight, Hottest Case

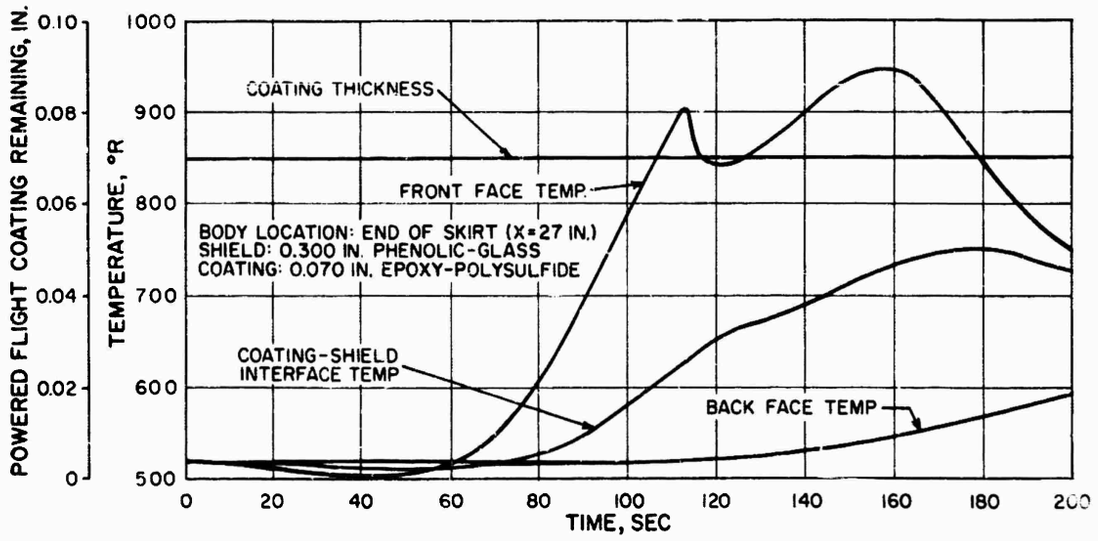

Figure 21. Shield Temperature and Ablation at End of Skirt During Powered Flight, Hottest Case

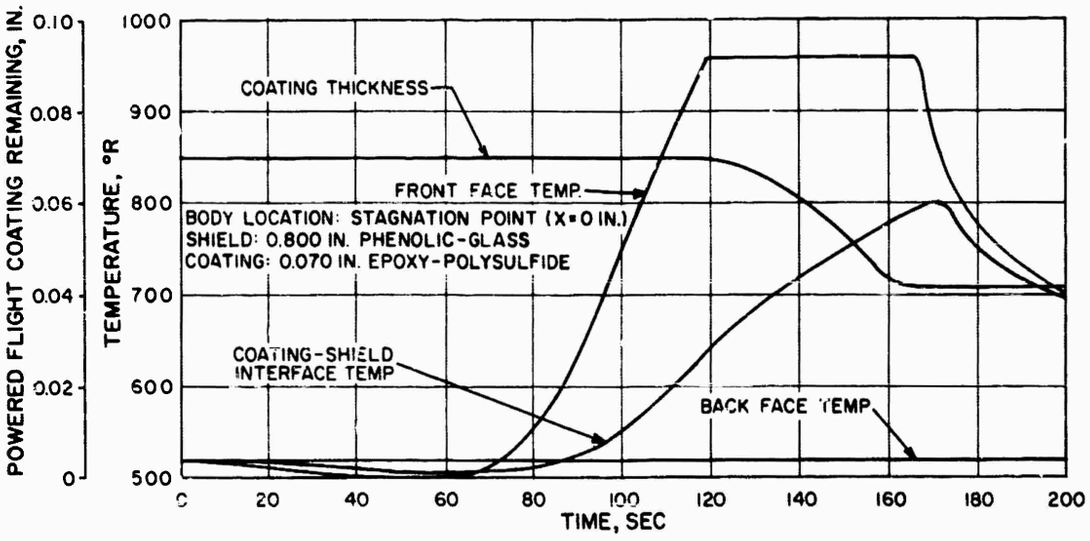

Figure 22. Shield Temperature and Ablation at Stagnation Point During Powered Flight, Coldest Case

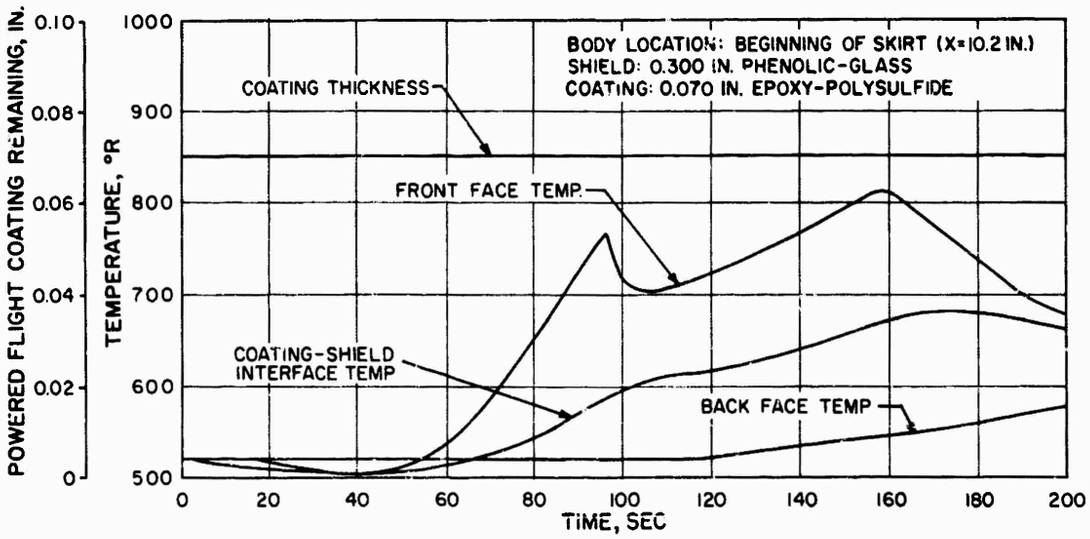

Figure 23. Shield Temperature and Ablation at Beginning of Skirt During Powered Flight, Coldest Case

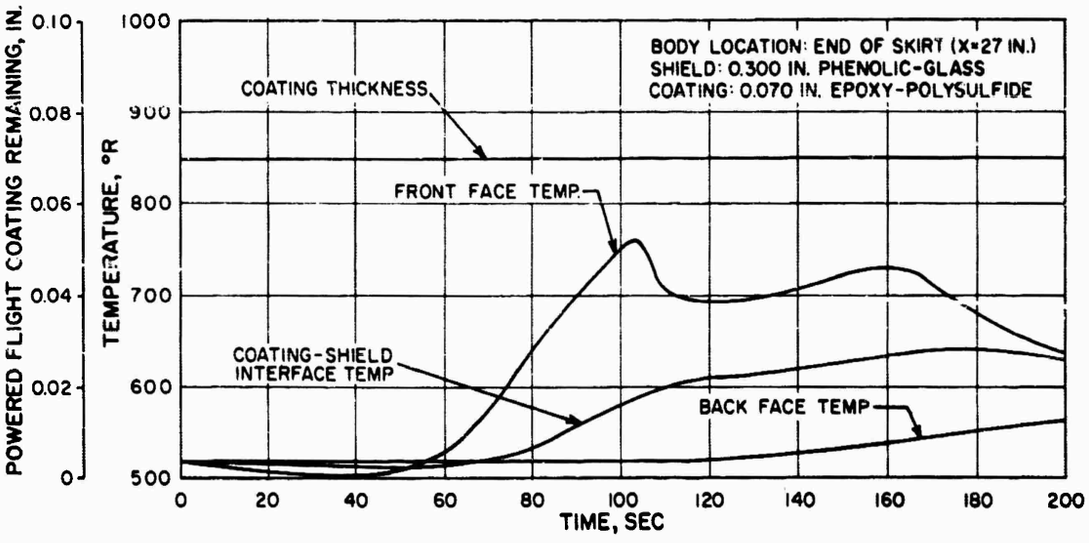

Figure 24. Shield Temperature and Ablation at End of Skirt During Powered Flight, Coldest Case

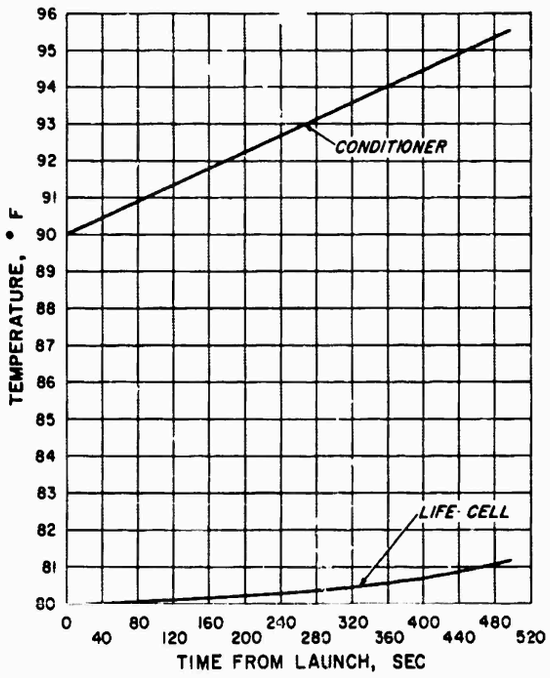

Figure 25. Life Cell and Conditioner Temperatures During Powered Flight, Hottest Case

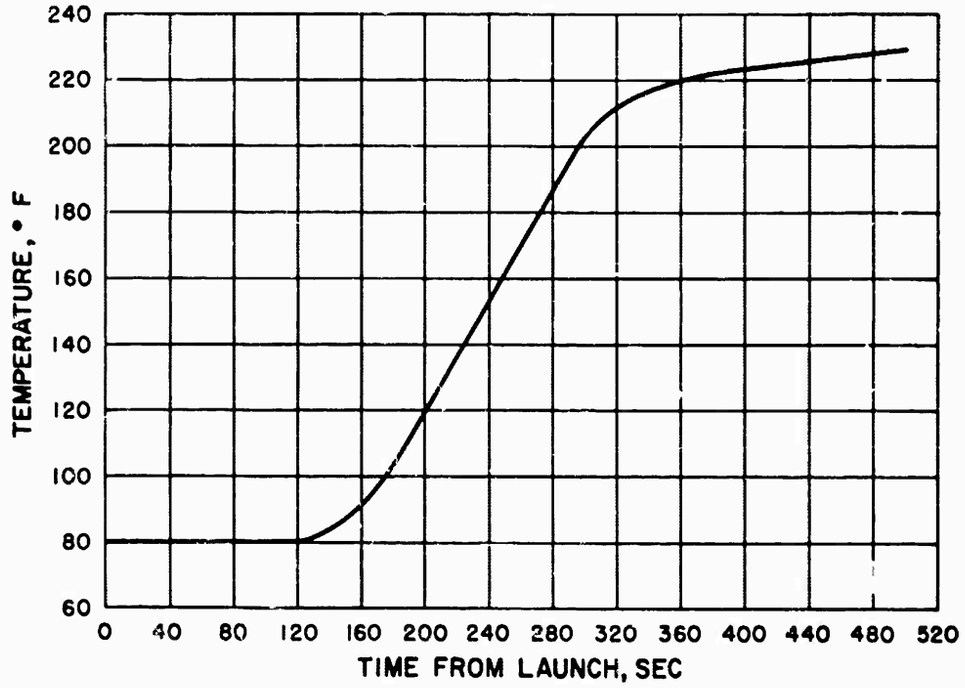

Figure 26. Magnesium Ring Temperature During Powered Flight, Hottest Case

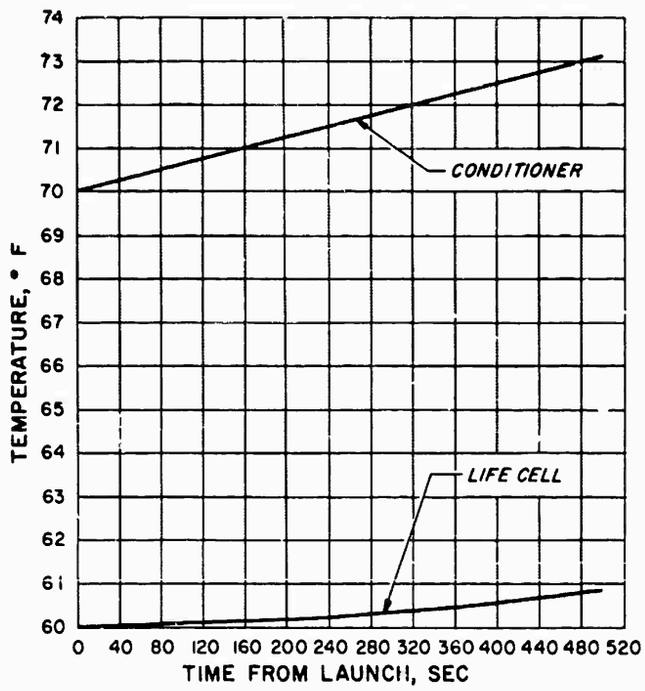

Figure 27. Life Cell and Conditioner Temperature During Powered Flight, Coldest Case

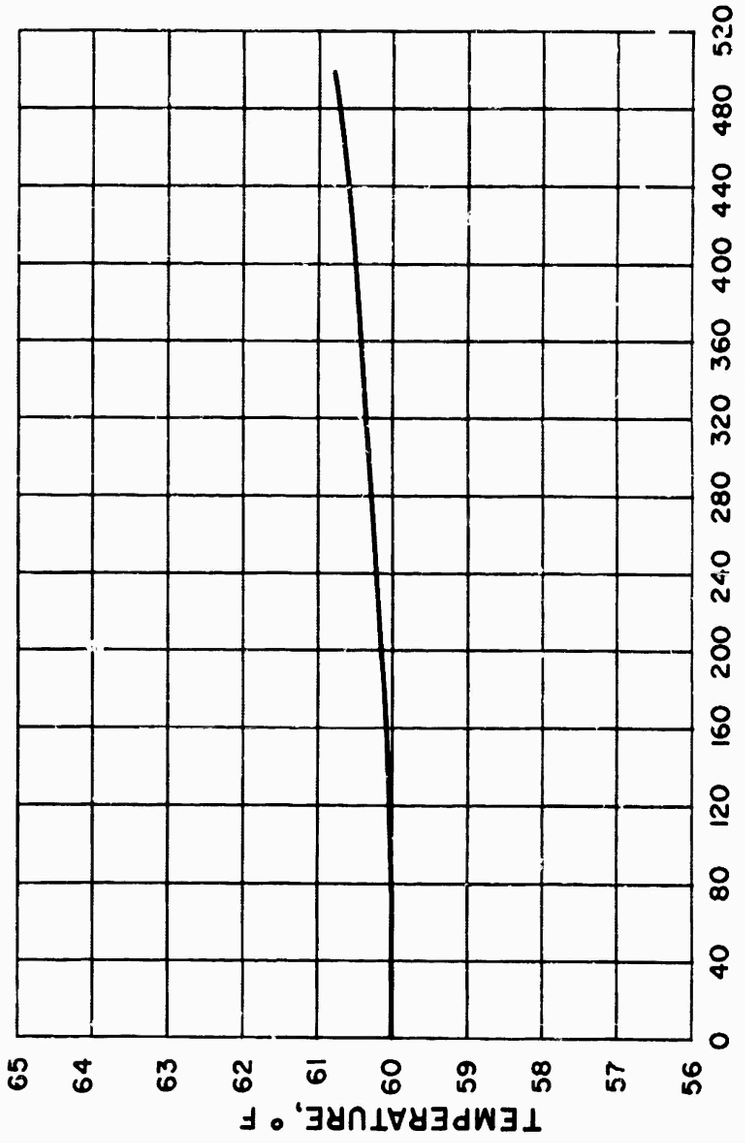

Figure 28. Beacon Battery Temperature During Powered Flight, Coldest Case

NOTE: ① CONVECTION IS ASSUMED TO BE NEGLIGIBLE
② NOT ALL RADIATIVE RESISTANCES ARE SHOWN
③ VALUES WITHIN ⬭ ARE HEAT CAPACITIES OF COMPONENTS IN BTU/°F
④ RESISTANCE VALUES ARE IN HR-° F/BTU

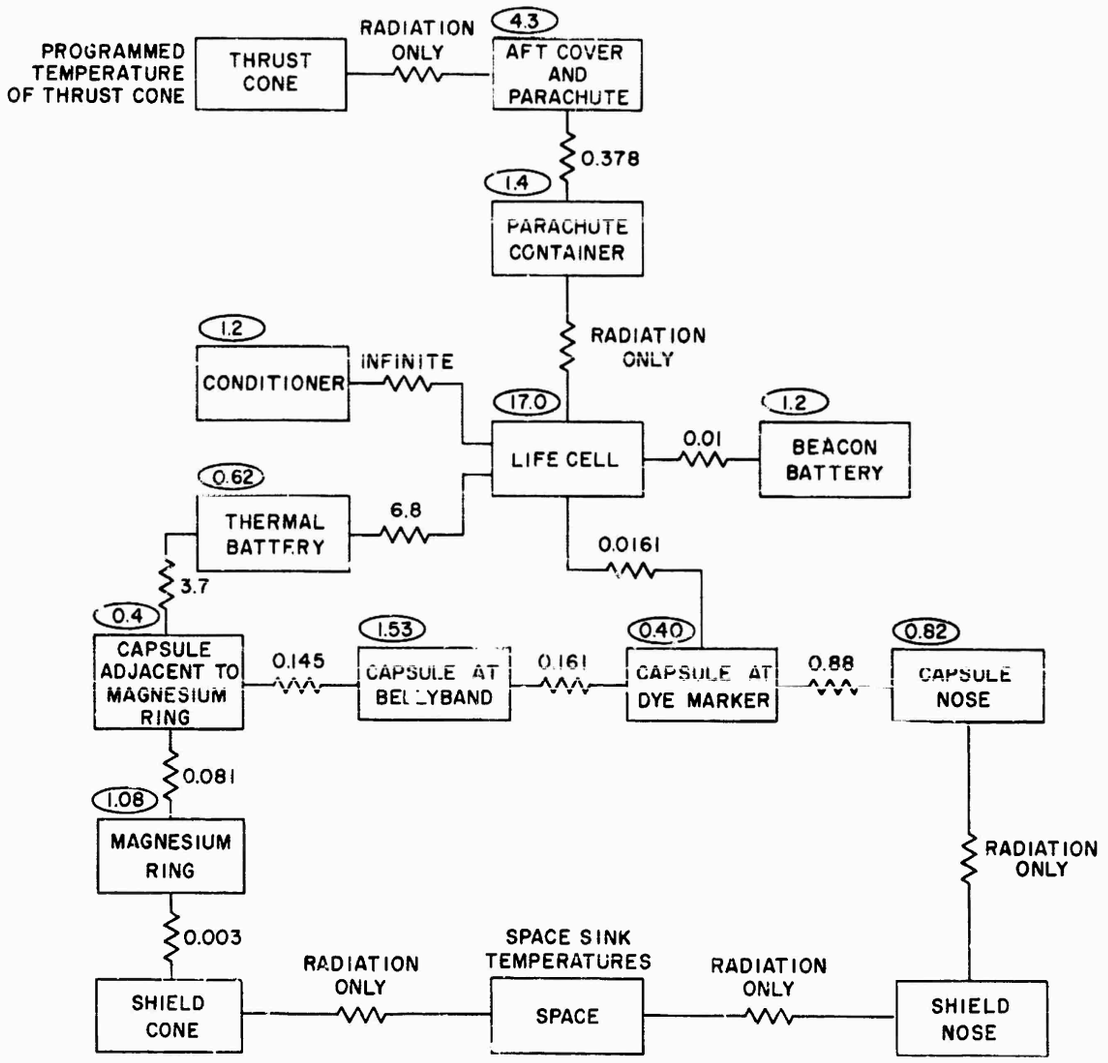

Figure 28. Simplified Electrical Circuit Analogous to Thermal Conduction Between Internal Components During Orbital Flight

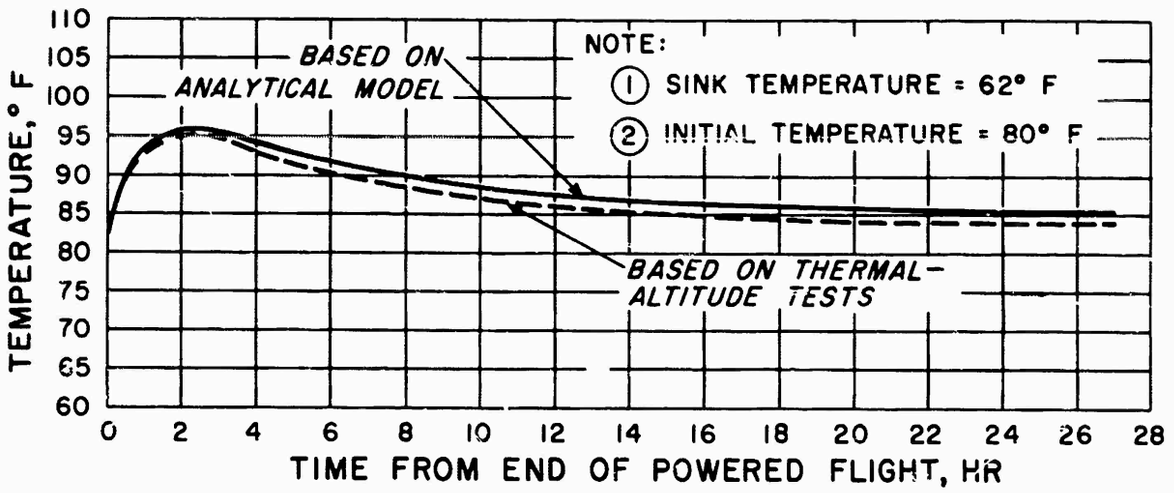

Figure 30. Life Cell Temperature During Orbital Flight, Hottest Case

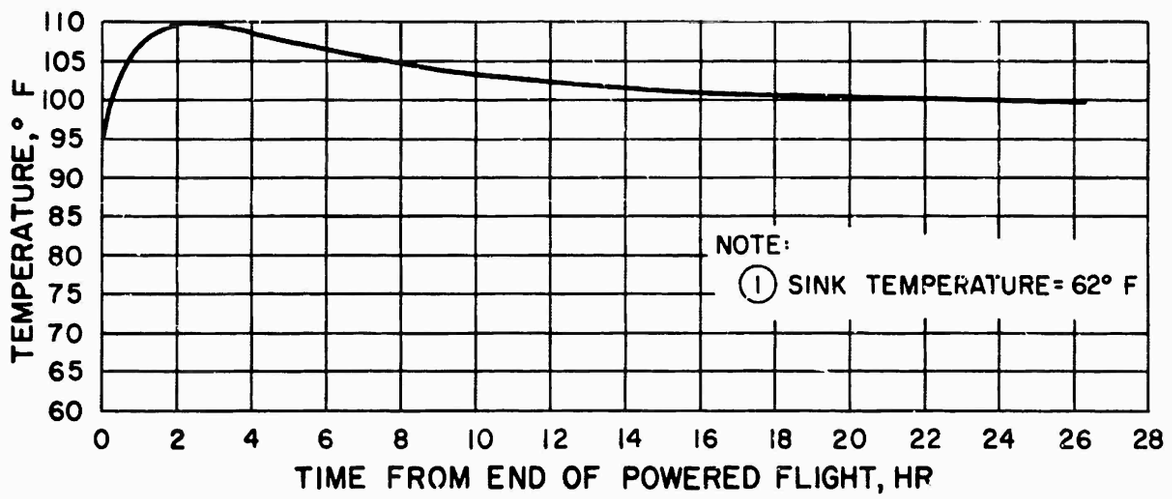

Figure 31. Conditioner Temperature During Orbital Flight, Hottest Case

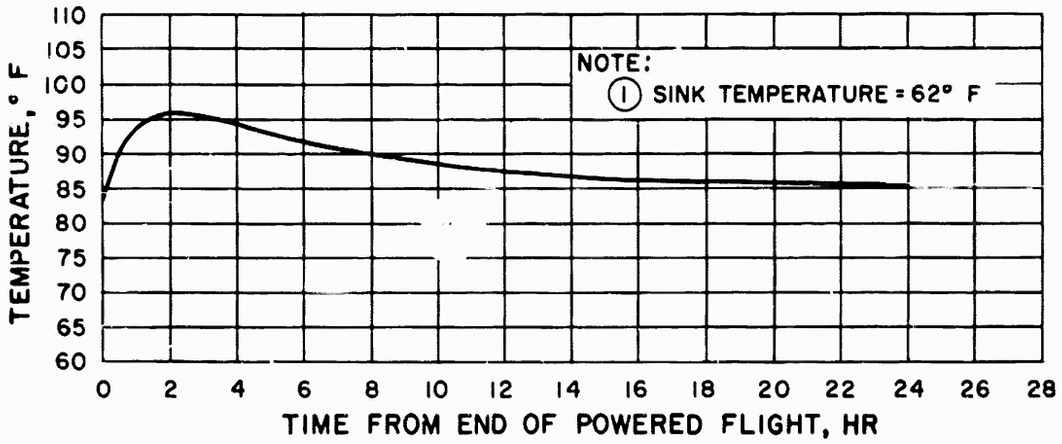

Figure 32. Beacon Battery Temperature During Orbital Flight, Hottest Case

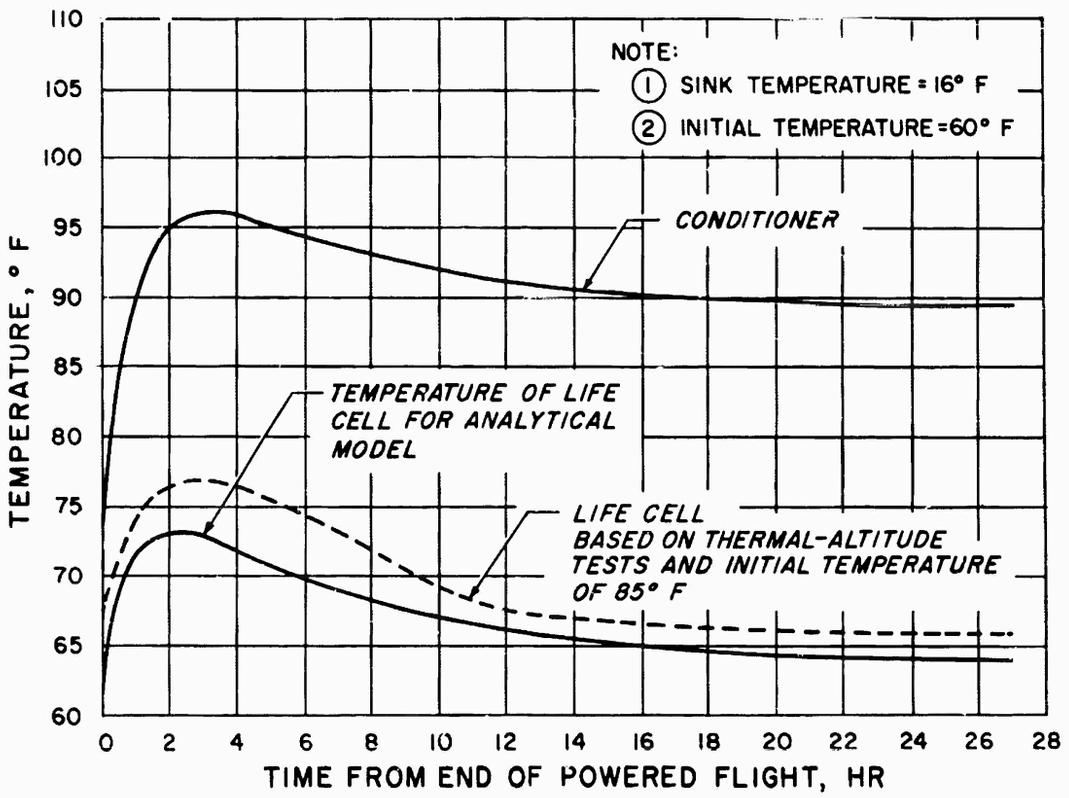

Figure 33. Life Cell and Conditioner Temperatures During Orbital Flight, Coldest Case

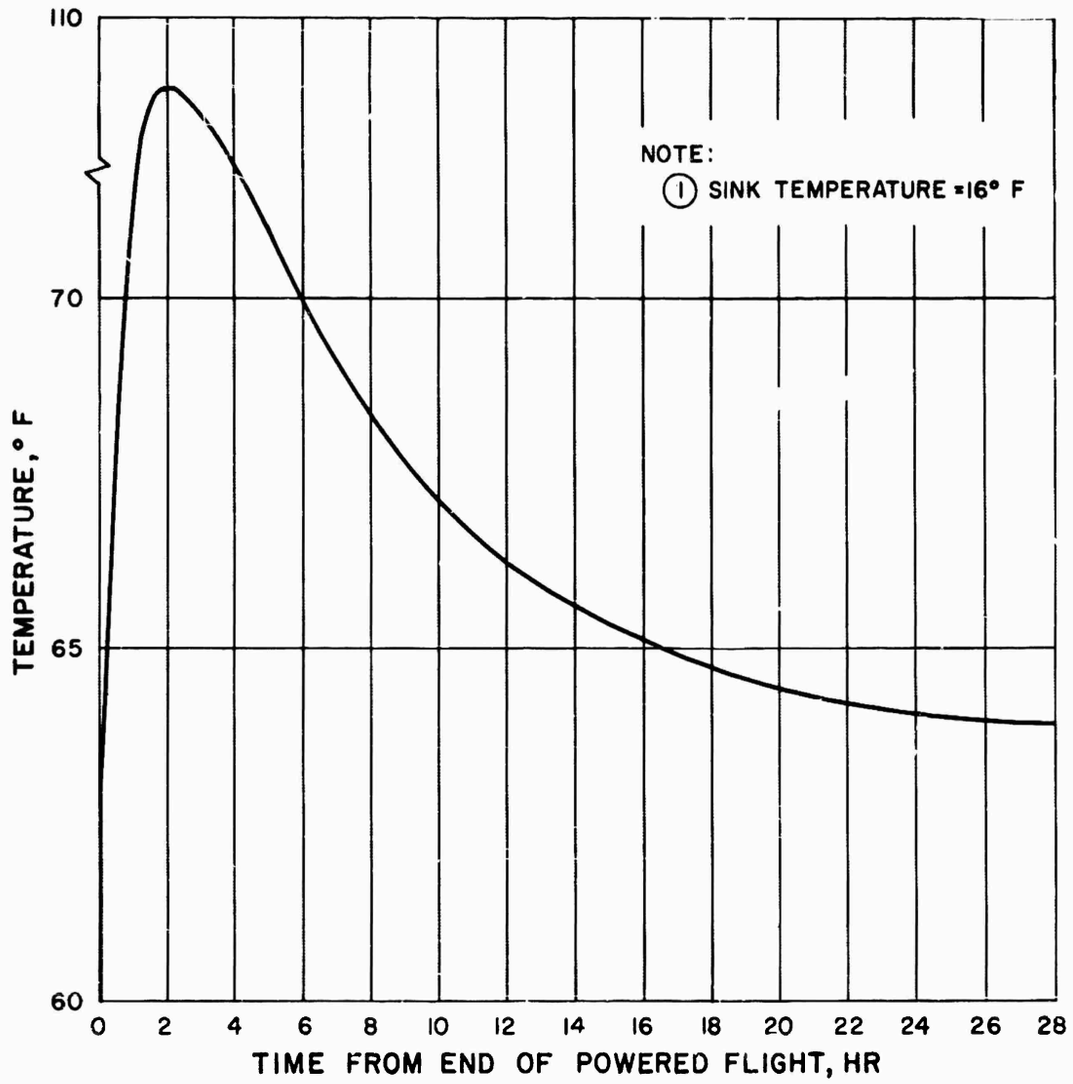

Figure 34. Beacon Battery Temperature During Orbital Flight, Coldest Case

NOTE: ① CONVECTION IS ASSUMED TO BE NEGLIGIBLE
② NOT ALL RADIATIVE RESISTANCES ARE SHOWN
③ VALUES WITHIN ⬭ ARE HEAT CAPACITIES OF COMPONENTS IN BTU/°F
④ RESISTANCE VALUES ARE IN HR-° F/BTU

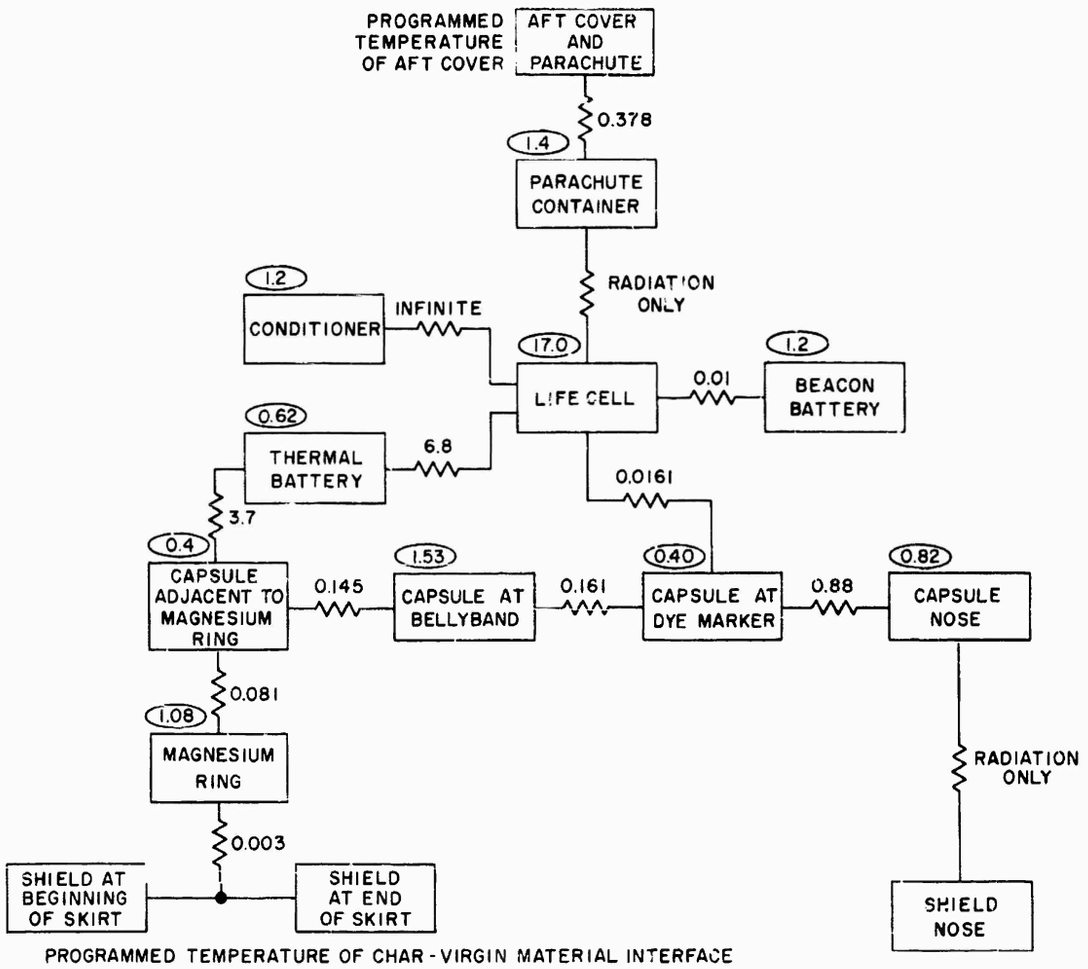

Figure 35. Simplified Electrical Circuit Analogous to Thermal Conduction Between Internal Components During Re-entry

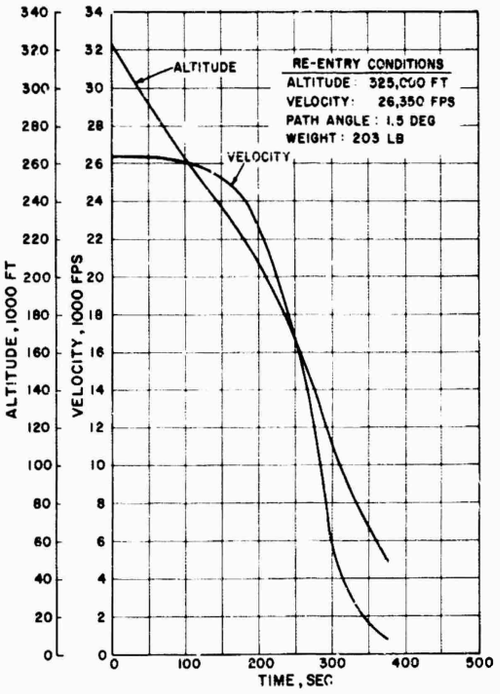

Figure 36. Trajectory During Re-entry, Hottest Case

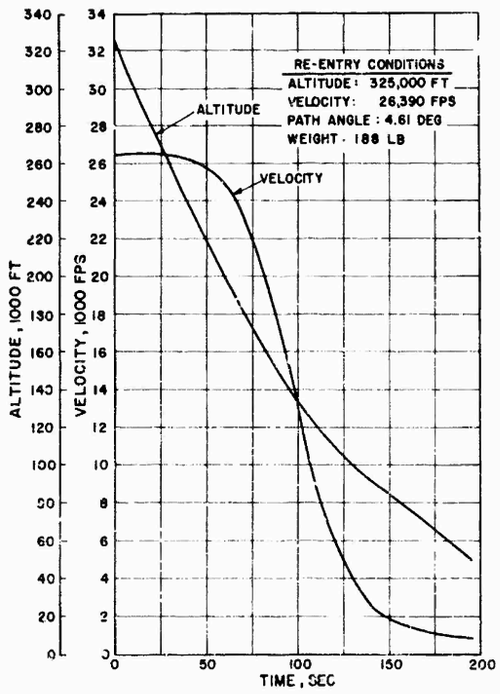

Figure 37. Trajectory During Re-entry, Coldest Case

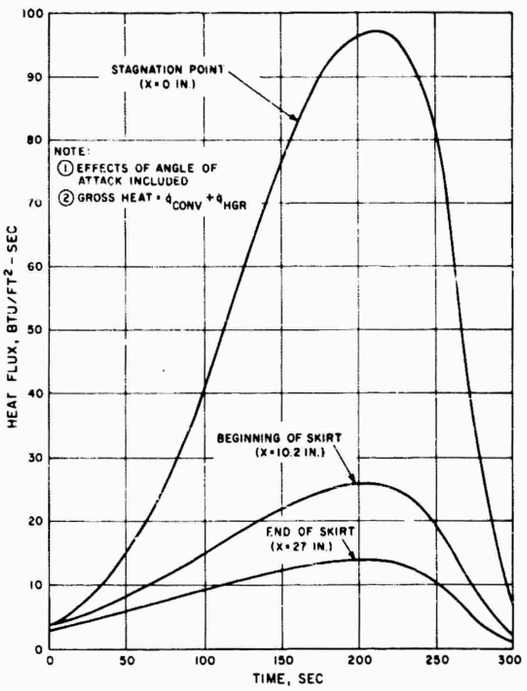

Figure 38. Gross Heat Fluxes to Body During Re-entry, Hottest Case

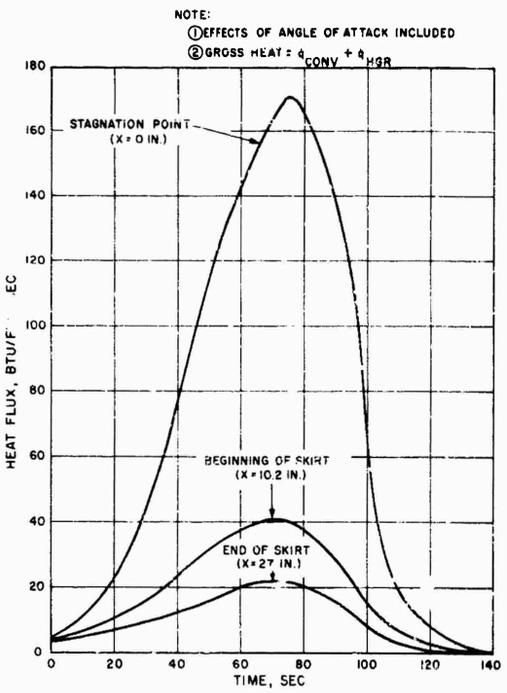

Figure 39. Gross Heat Fluxes to Body During Re-entry, Coldest Case

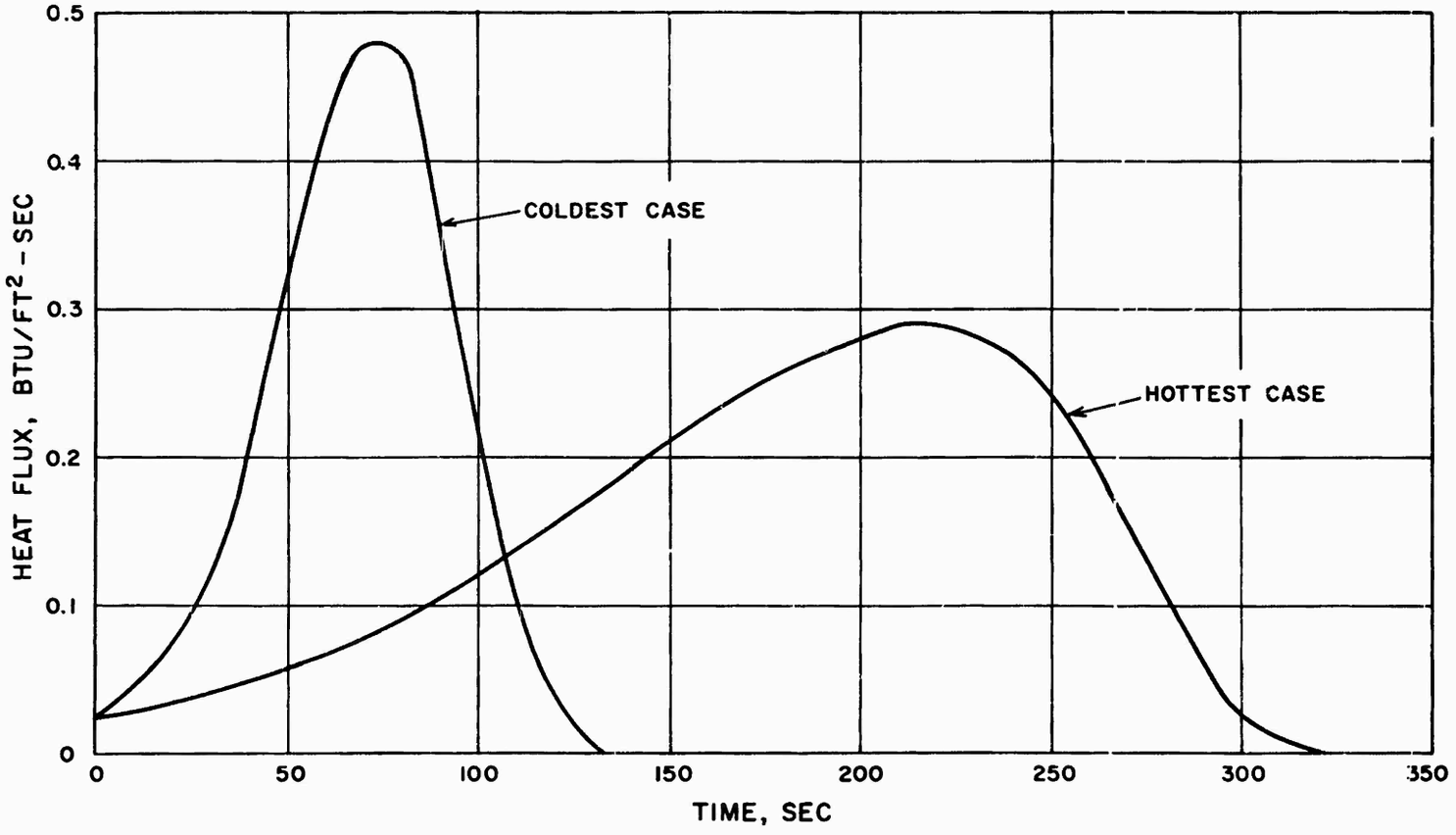

Figure 40. Wake Heat Fluxes During Re-entry

CONFIDENTIAL

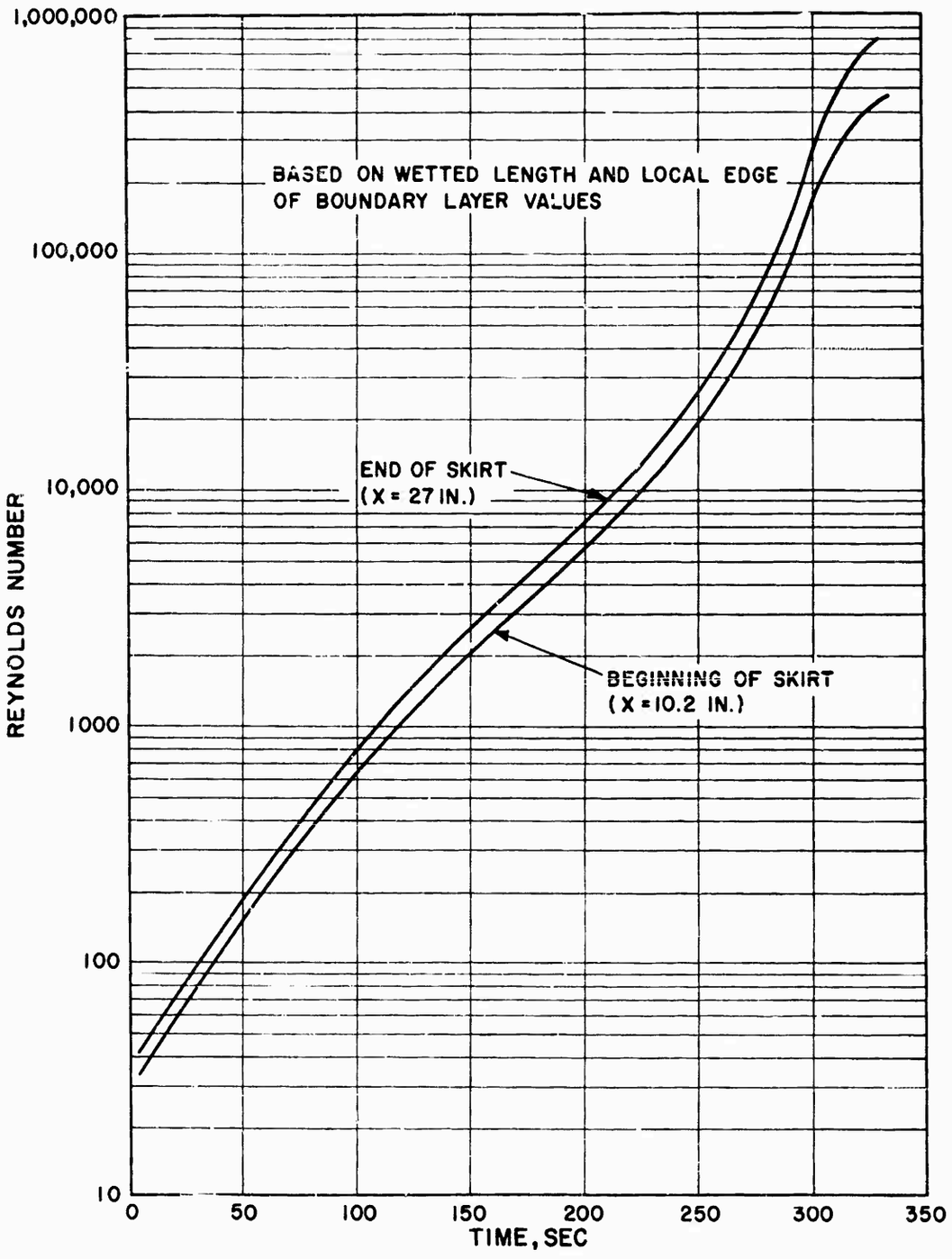

Figure 41. Reynolds Number During Re-entry, Hottest Case

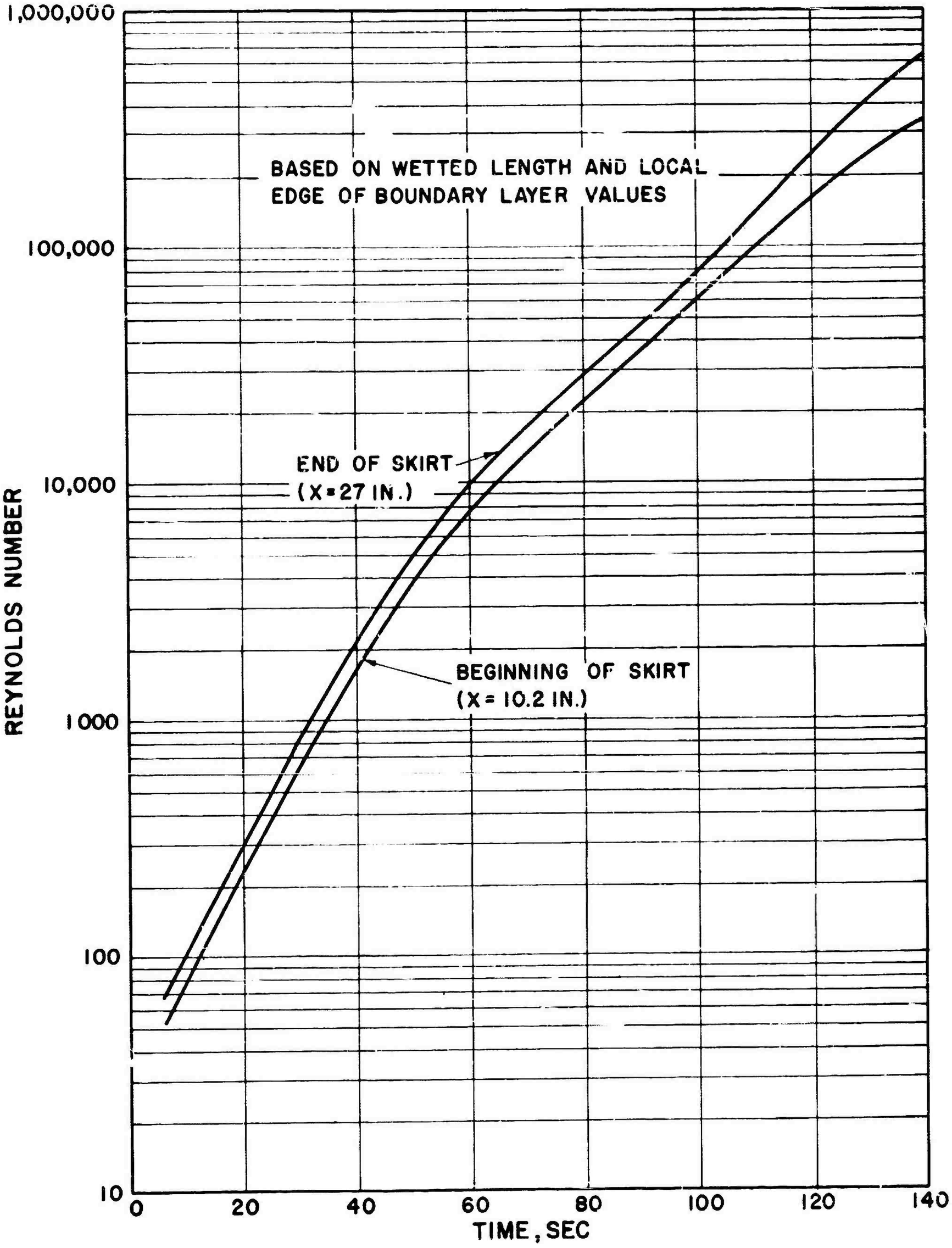

Figure 42. Reynolds Number During Re-entry, Coldest Case

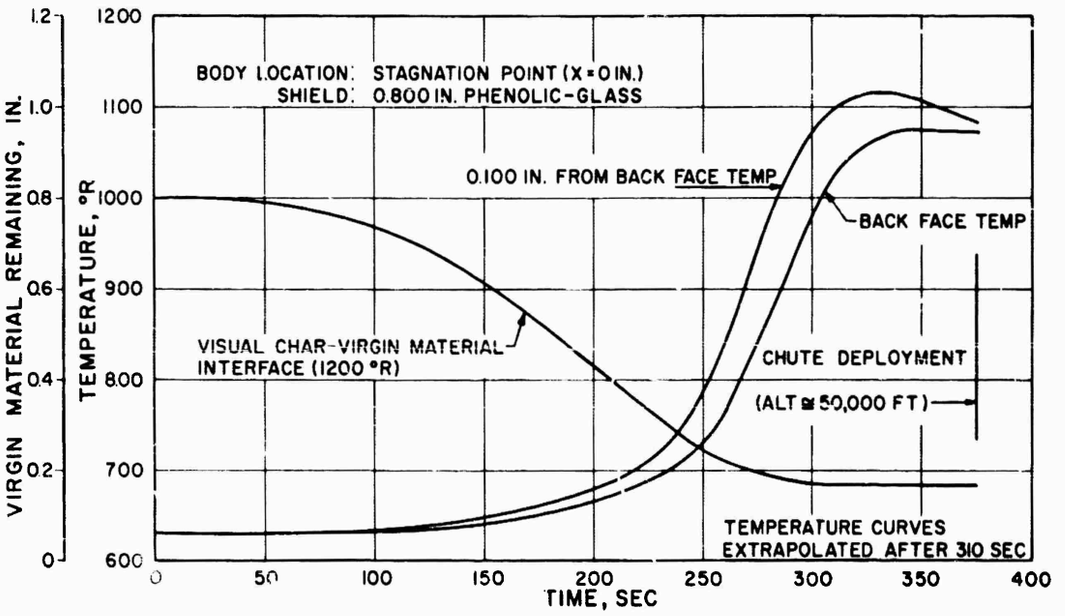

Figure 43. Shield Temperature and Char at Stagnation Point During Re-entry, Hottest Case

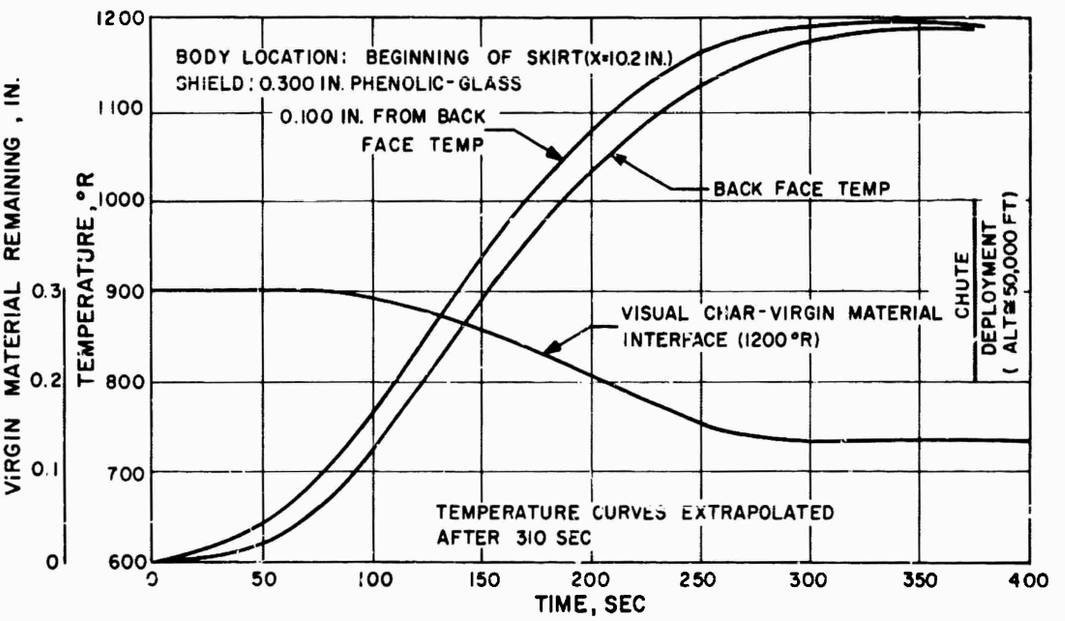

Figure 44. Shield Temperature and Char at Beginning of Skirt During Re-entry, Hottest Case

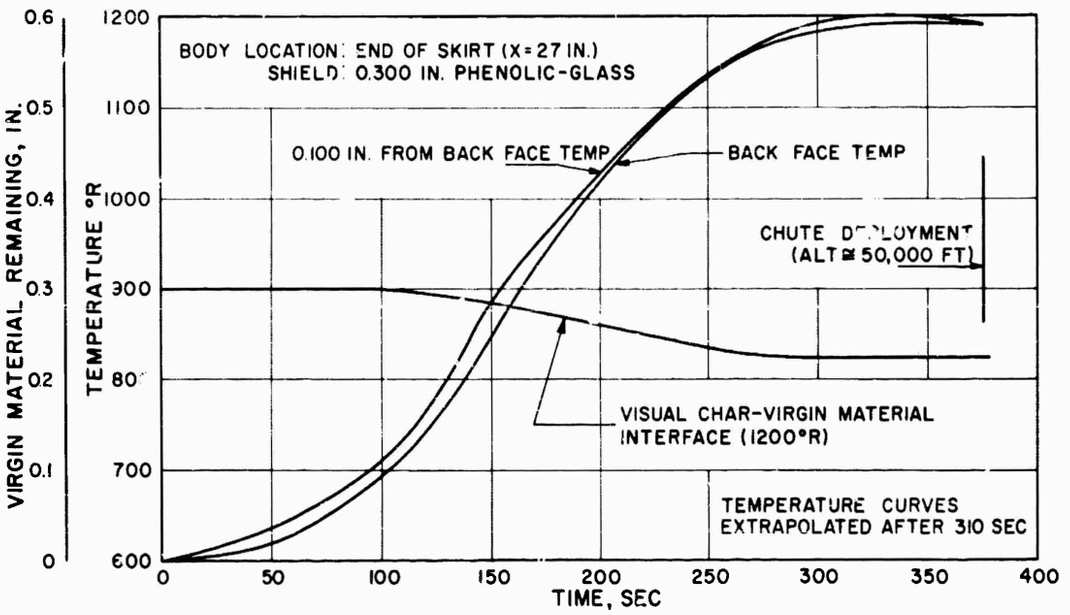

Figure 45. Shield Temperature and Char at End of Skirt During Re-entry, Hottest Case

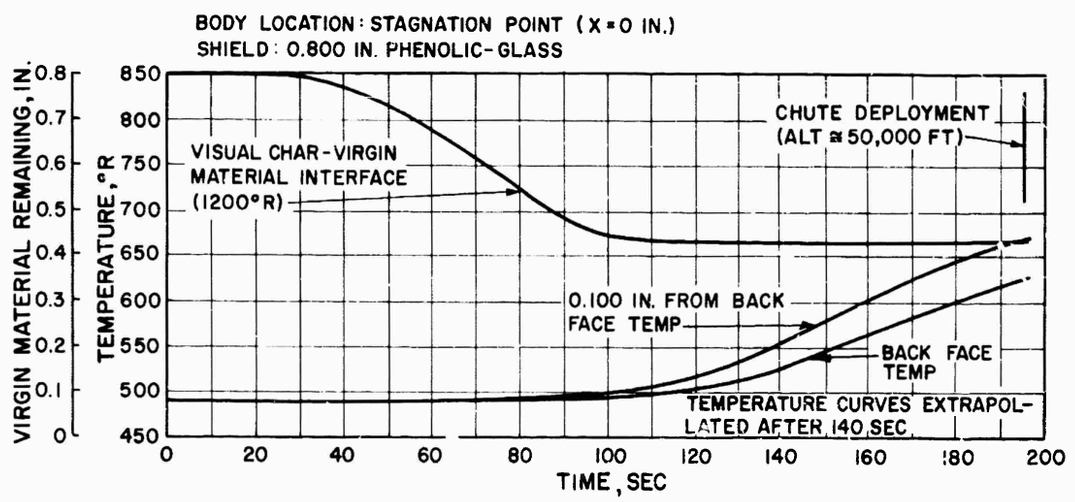

Figure 46. Shield Temperature and Char at Stagnation Point During Re-entry, Coldest Case

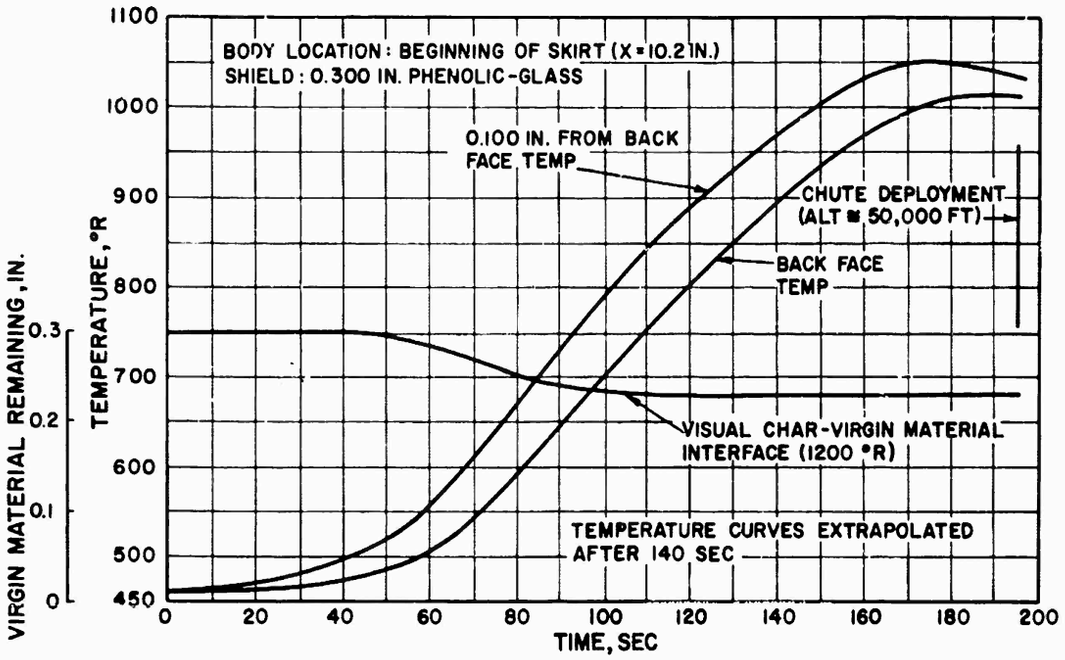

Figure 47. Shield Temperature and Char at Beginning of Skirt During Re-entry, Coldest Case

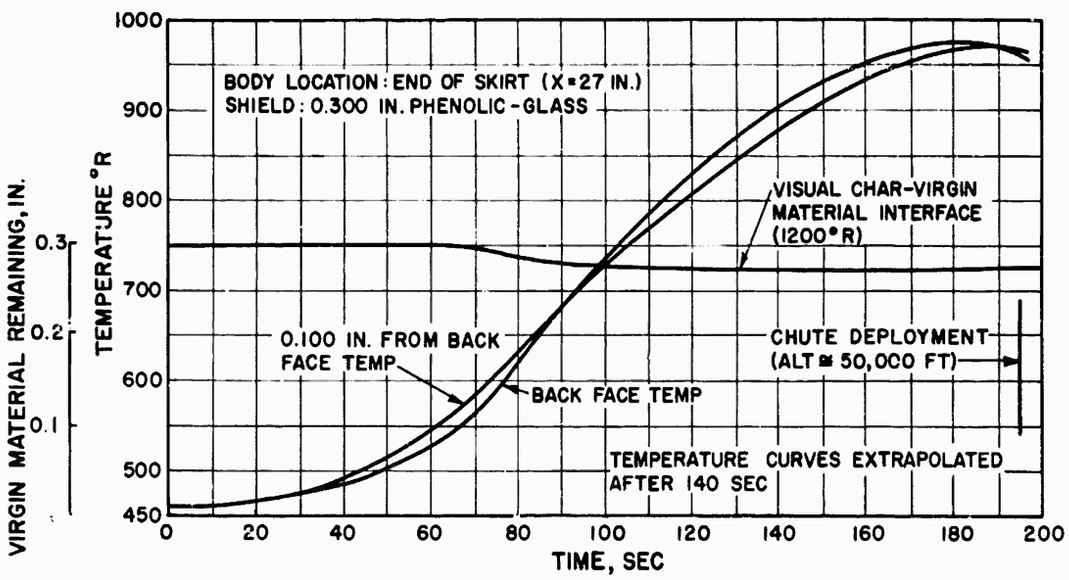

Figure 48. Shield Temperature and Char at End of Skirt During Re-entry, Coldest Case

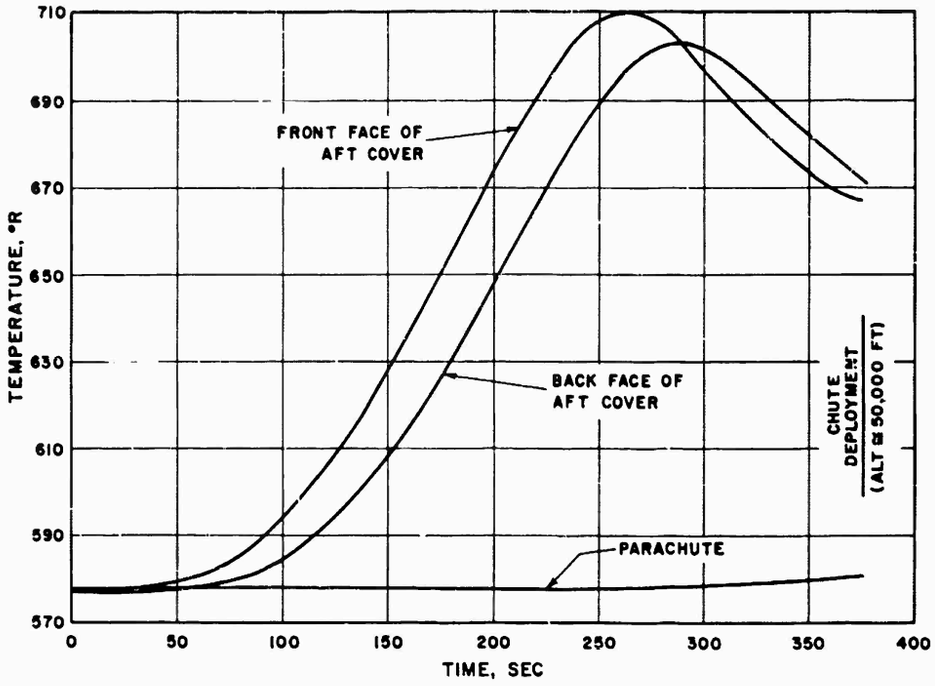

Figure 49. Temperature History of Parachute and Aft Cover, Hottest Case

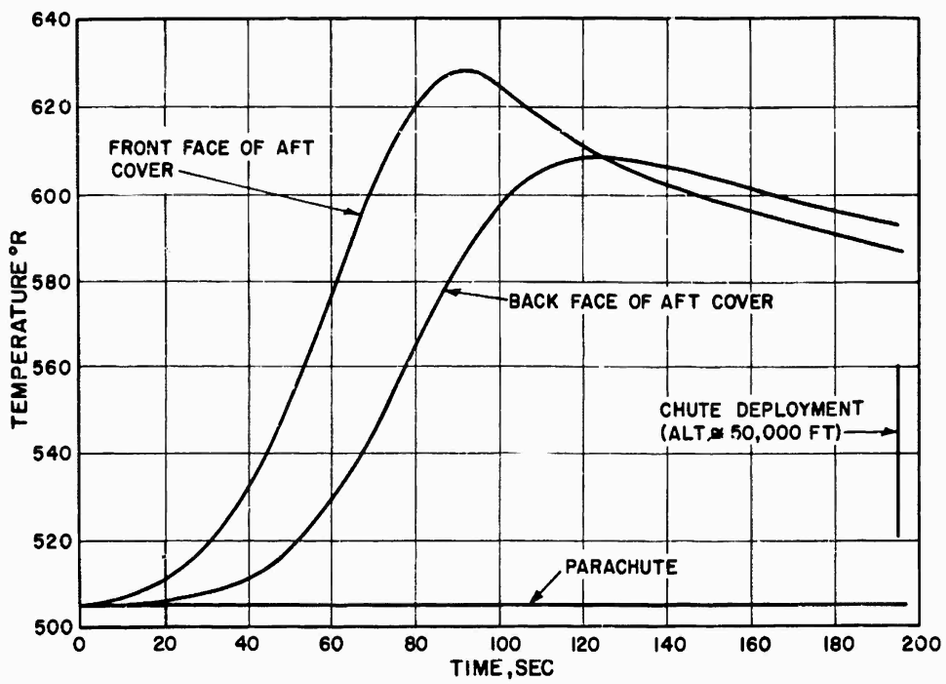

Figure 50. Temperature History of Parachute and Aft Cover, Coldest Case

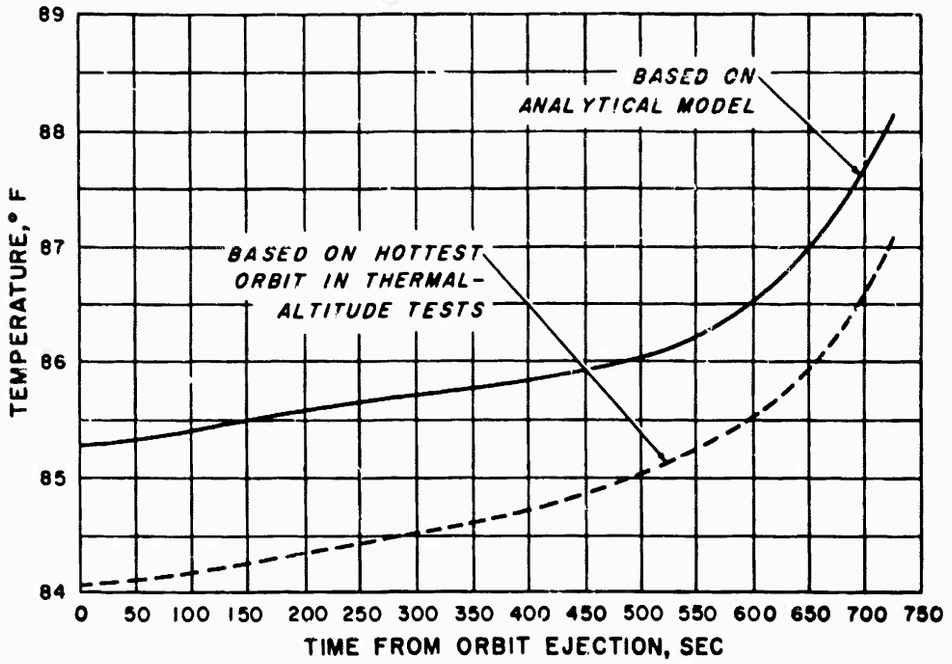

Figure 51. Life Cell Temperature During Re-entry, Hottest Case

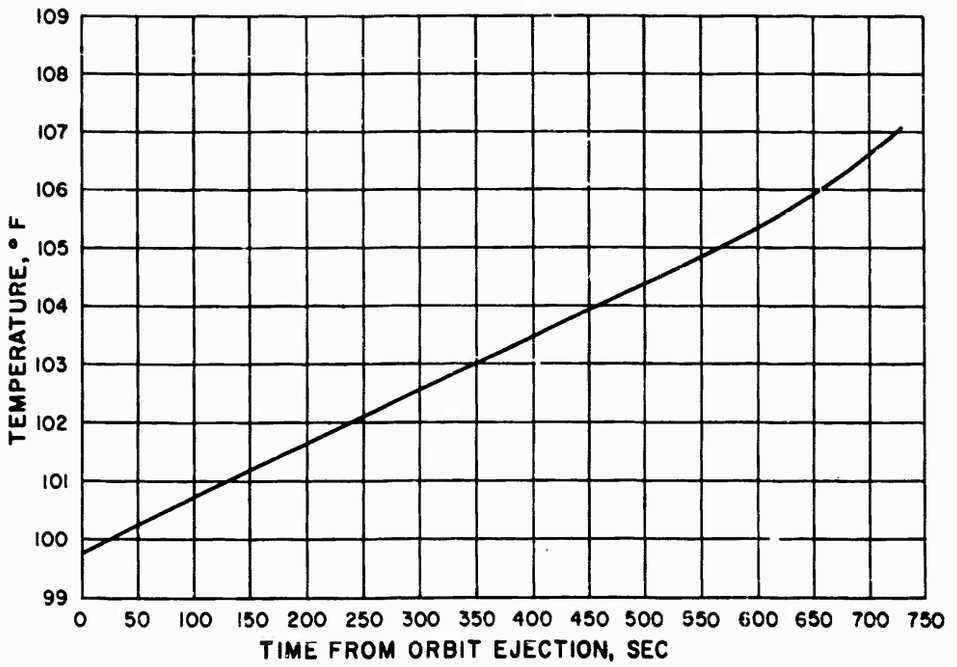

Figure 52. Conditioner Temperature During Re-entry, Hottest Case

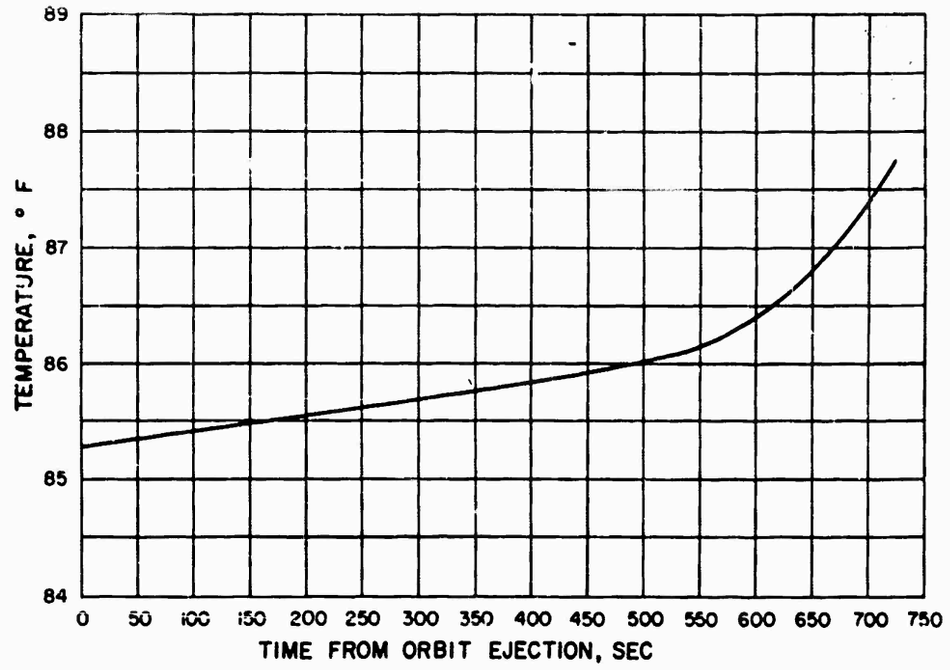

Figure 53. Beacon Battery Temperature During Re-entry, Hottest Case

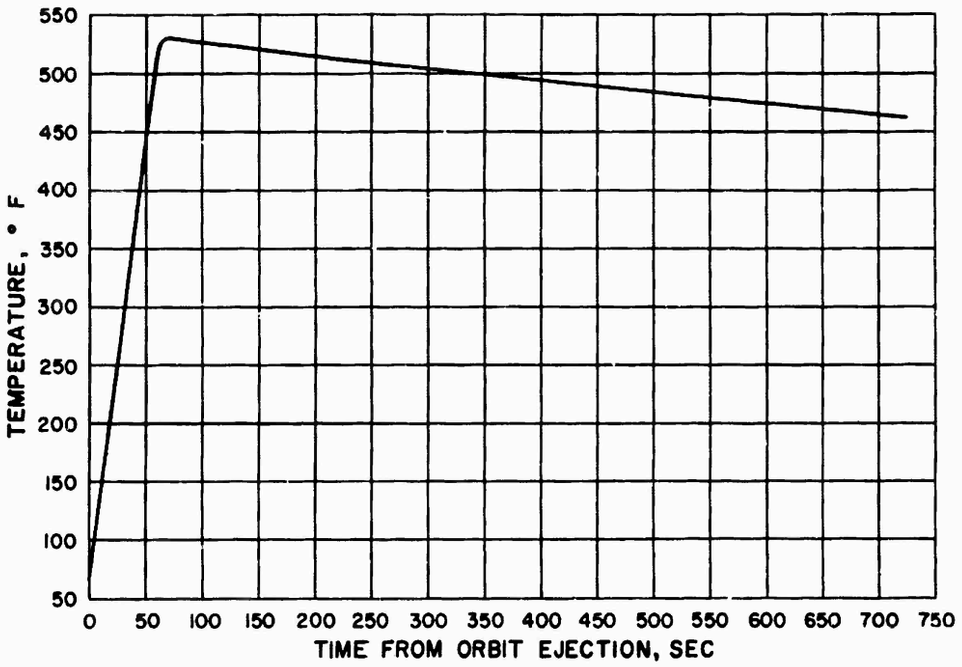

Figure 54. Thermal Battery Temperature During Re-entry, Hottest Case

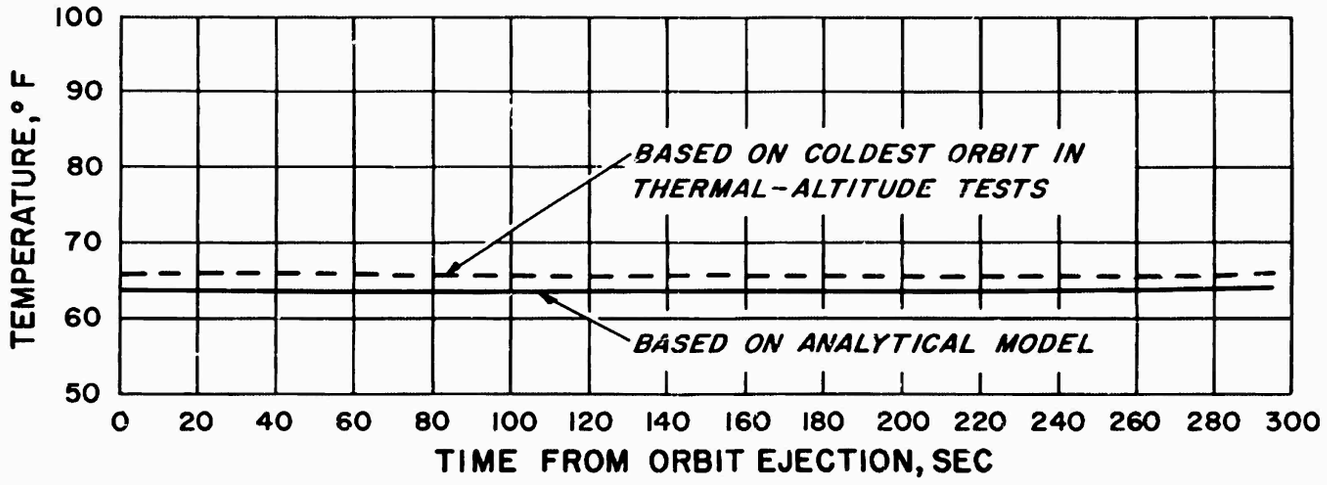

Figure 55. Life Cell Temperature During Re-entry, Coldest Case

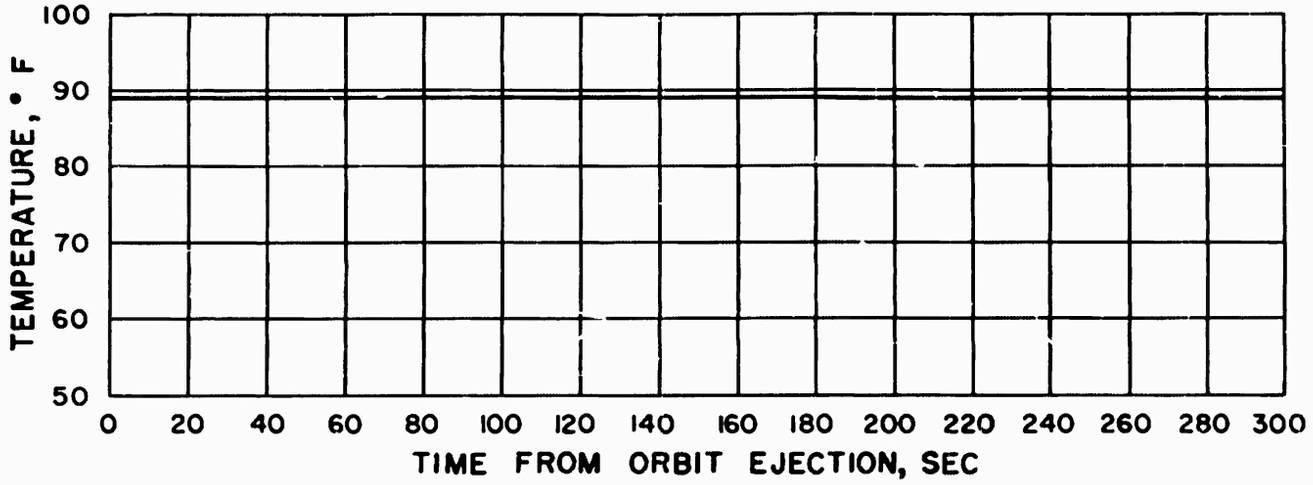

Figure 56. Conditioner Temperature During Re-entry, Coldest Case

CONFIDENTIAL

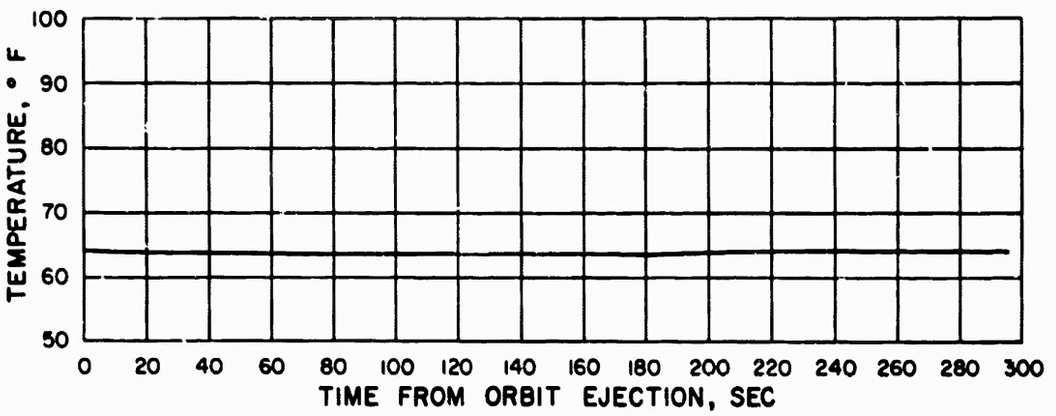

Figure 57. Beacon Battery Temperature During Re-entry, Coldest Case

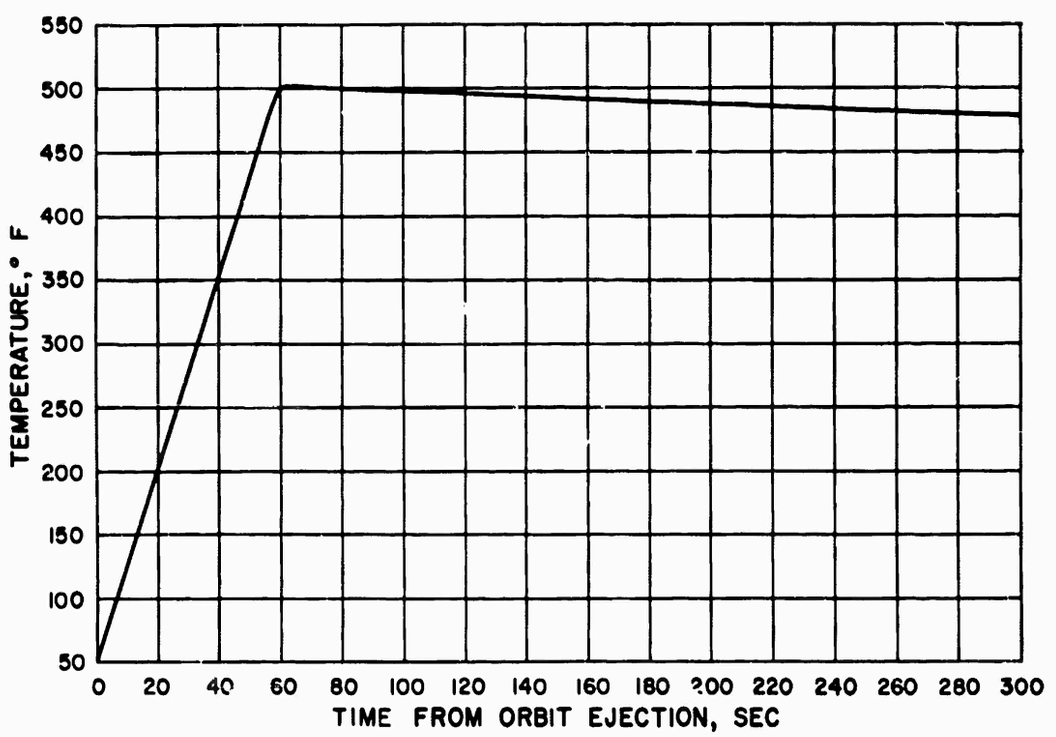

Figure 58. Thermal Battery Temperature During Re-entry, Coldest Case

CONFIDENTIAL

NOTE: ① CONVECTION EFFECTS ARE INCLUDED
② NOT ALL RADIATIVE RESISTANCES ARE SHOWN
③ VALUES WITHIN ⬭ ARE HEAT CAPACITIES OF COMPONENTS IN BTU/°F
④ RESISTANCE VALUES ARE IN HR-° F/BTU

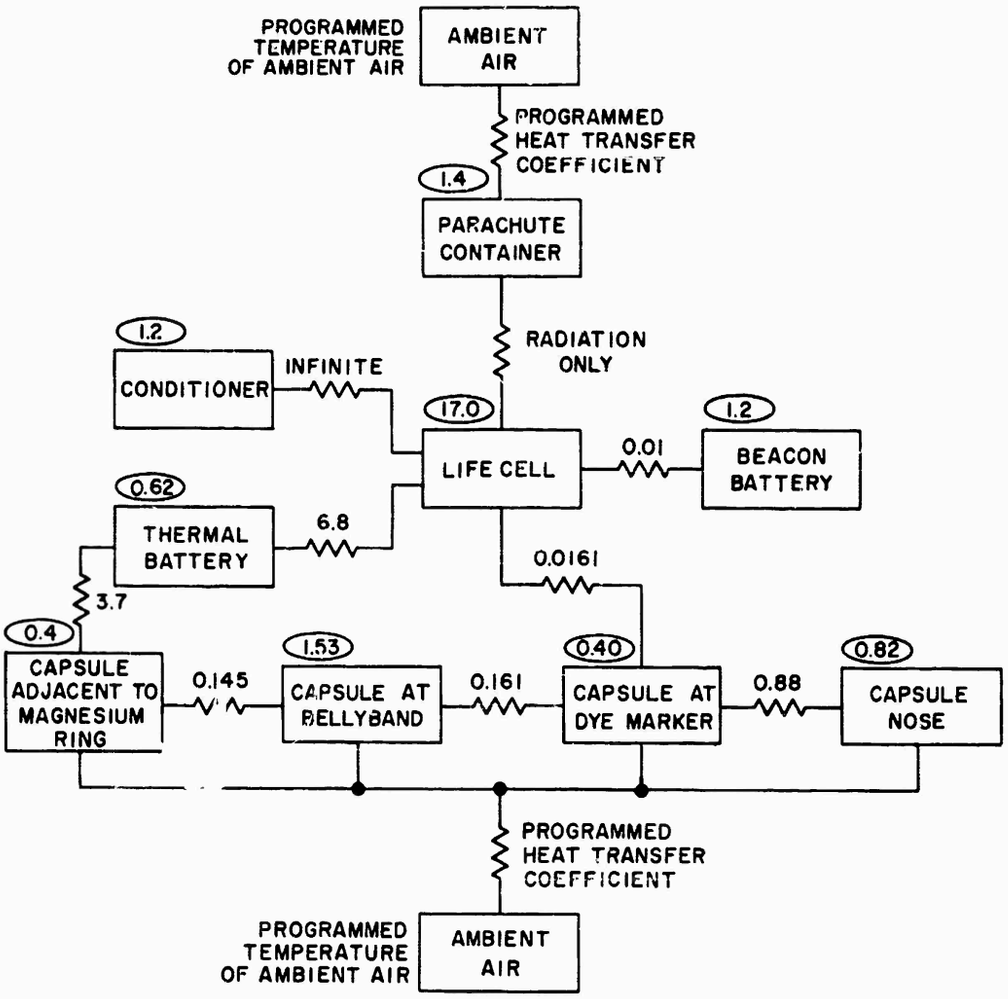

Figure 59. Simplified Electrical Circuit Analogous to Thermal Conduction Between Internal Components During Parachute Descent and Air Pickup

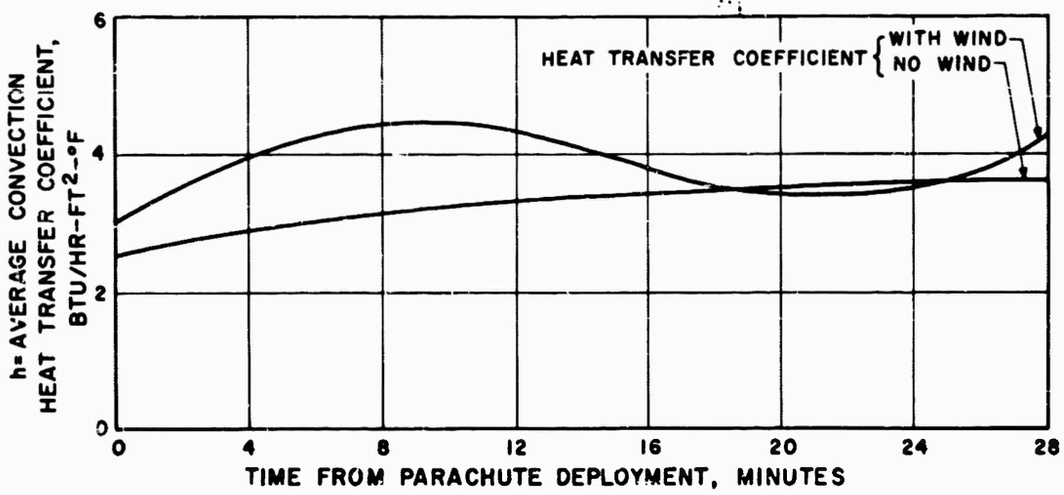

Figure 60. Heat Transfer Coefficients During Parachute Descent

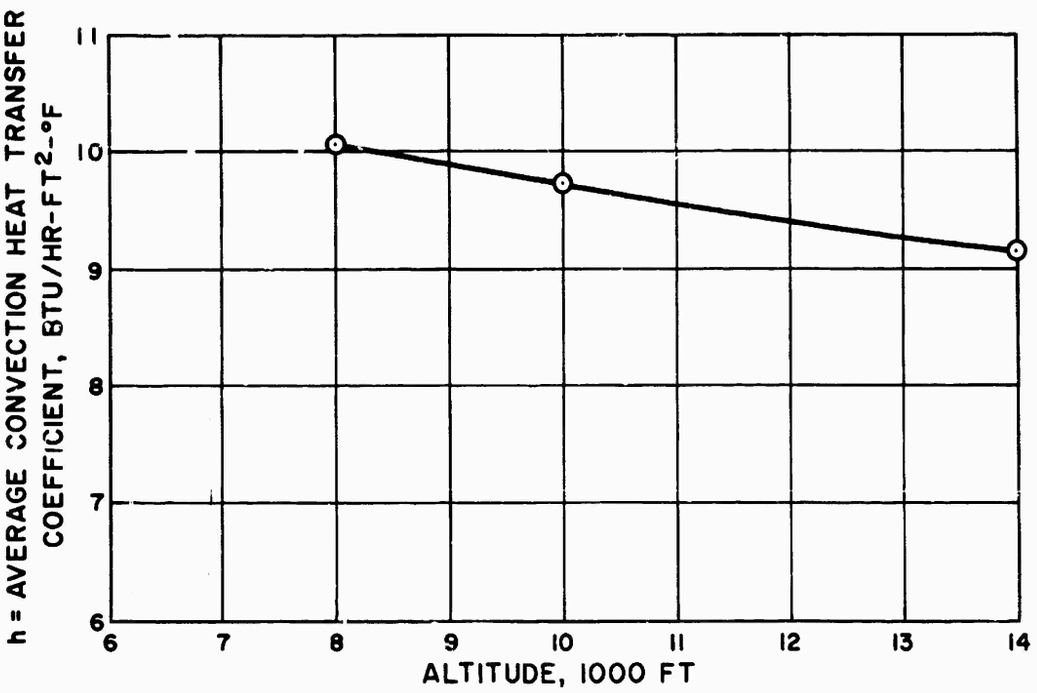

Figure 61. Heat Transfer Coefficient During Air Pickup

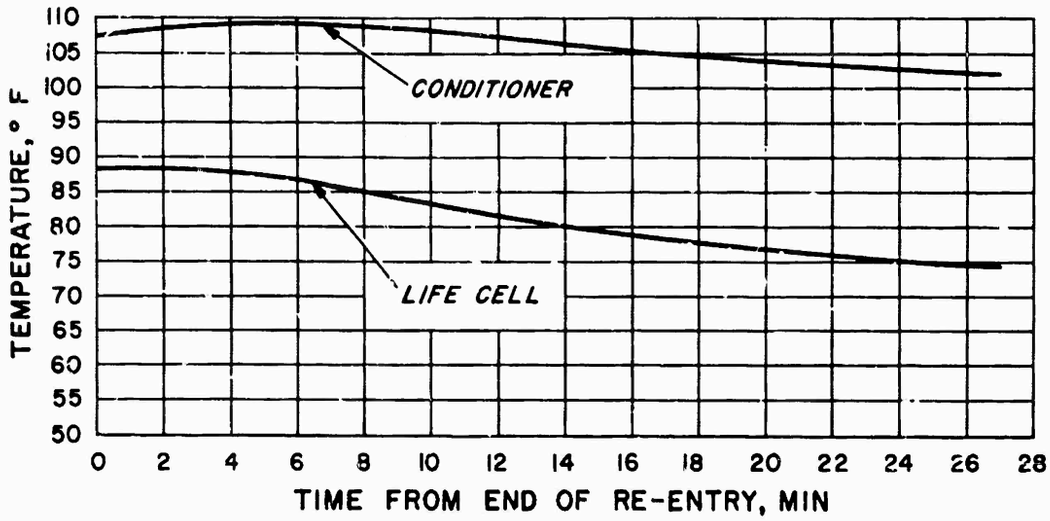

Figure 62. Life Cell and Conditioner Temperature During Parachute Descent, Hottest Case

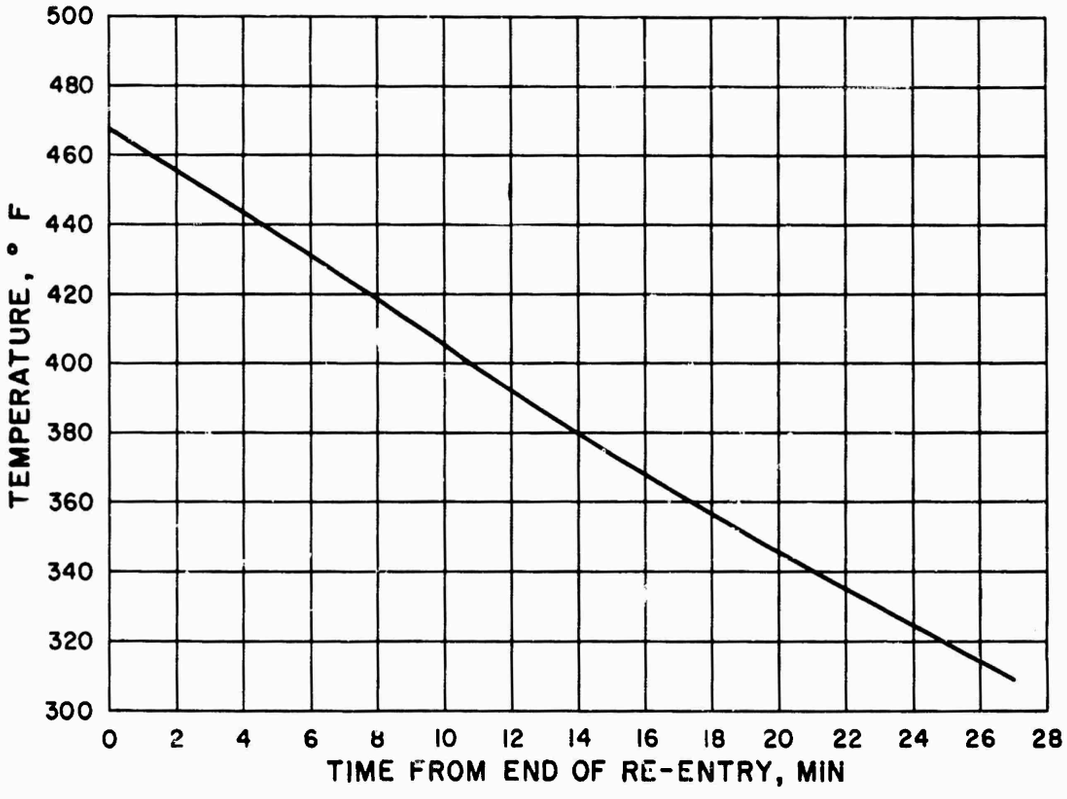

Figure 63. Thermal Battery Temperature During Parachute Descent, Hottest Case

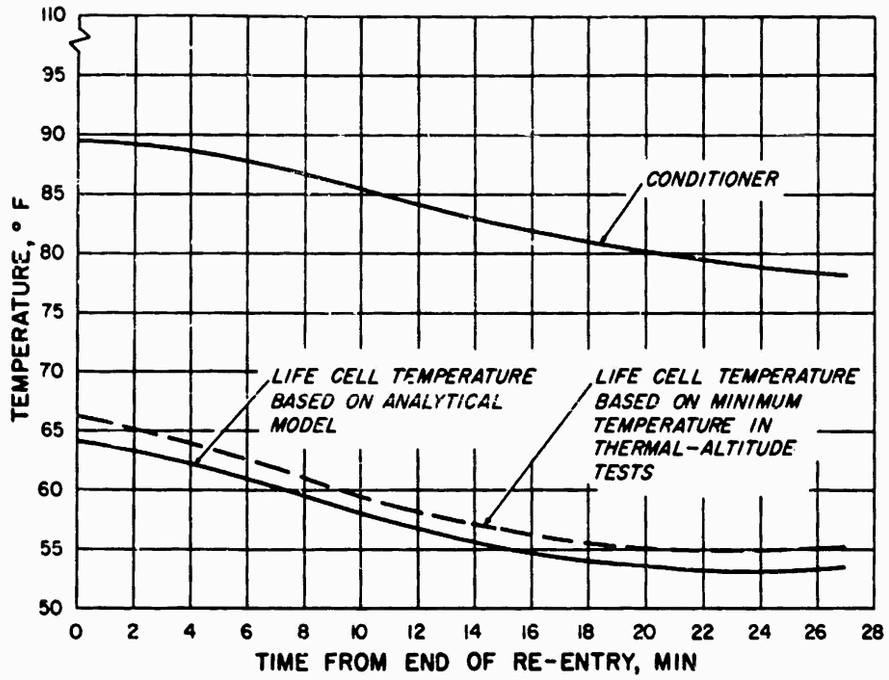

Figure 64. Life Cell and Conditioner Temperatures During Parachute Descent, Coldest Case

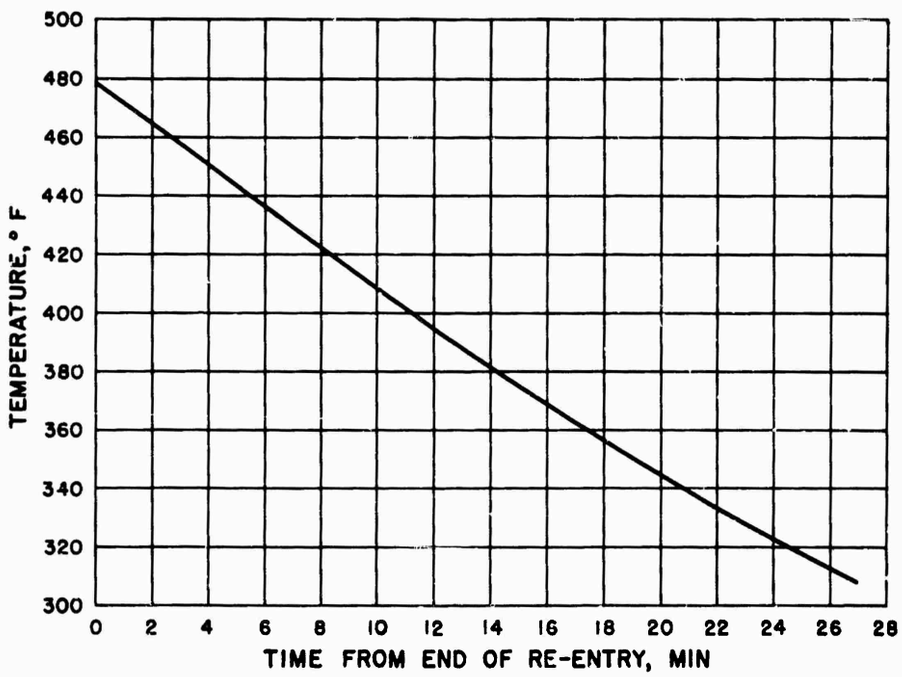

Figure 65. Thermal Battery Temperature During Parachute Descent, Coldest Case

CONFIDENTIAL

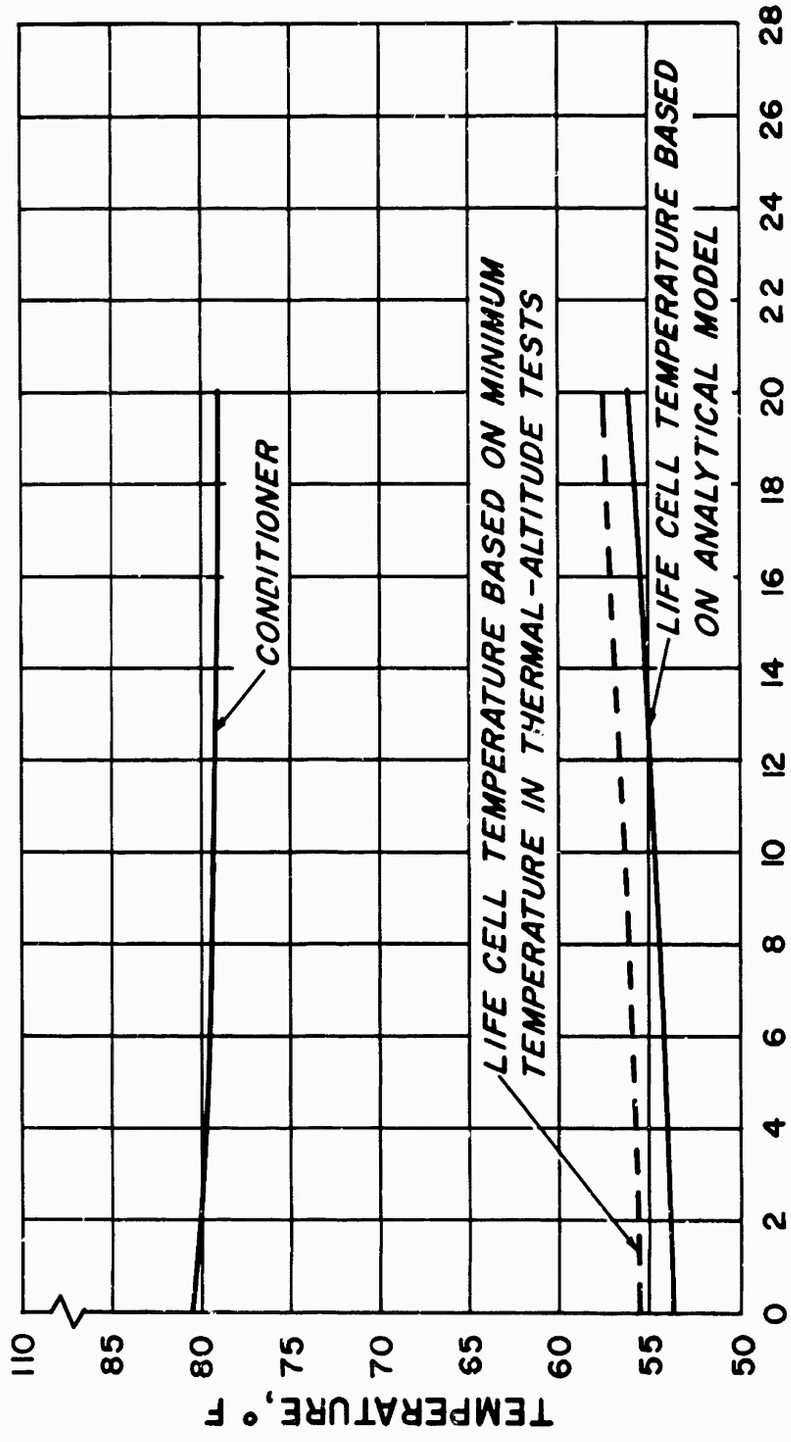

Figure 66. Life Cell and Conditioner Temperatures During Air Pickup, Coldest Case

CONFIDENTIAL

NOTE: ① CONVECTION EFFECTS ARE INCLUDED
② NOT ALL RADIATIVE RESISTANCES ARE SHOWN
③ VALUES WITHIN ⬭ ARE HEAT CAPACITIES OF COMPONENTS IN BTU/°F
④ RESISTANCE VALUES ARE IN HR-° F/BTU

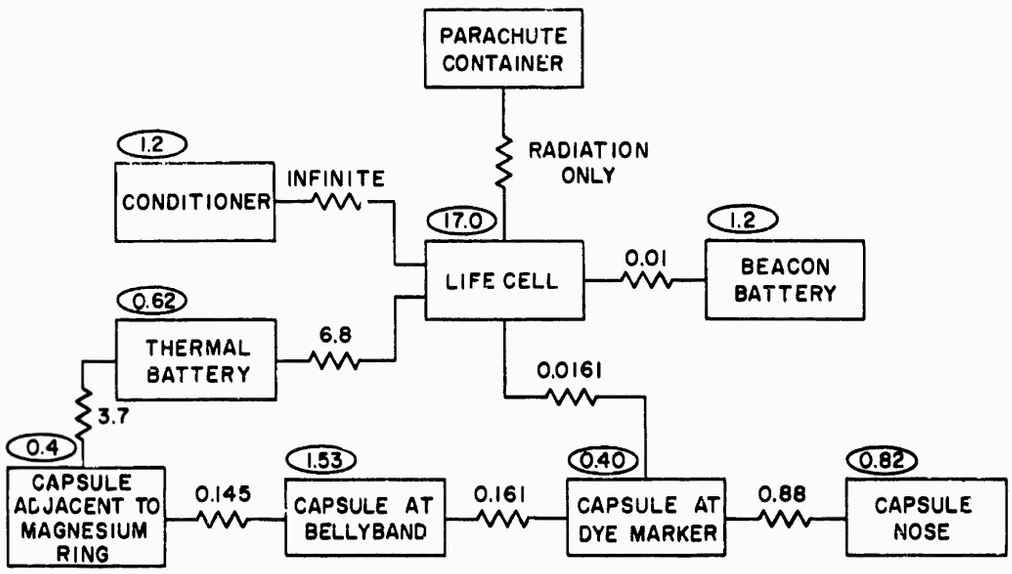

PROGRAMMED TEMPERATURE OF CAPSULE

Figure 67. Simplified Electrical Circuit Analogous to Thermal Conduction Between Internal Components During Water Flotation

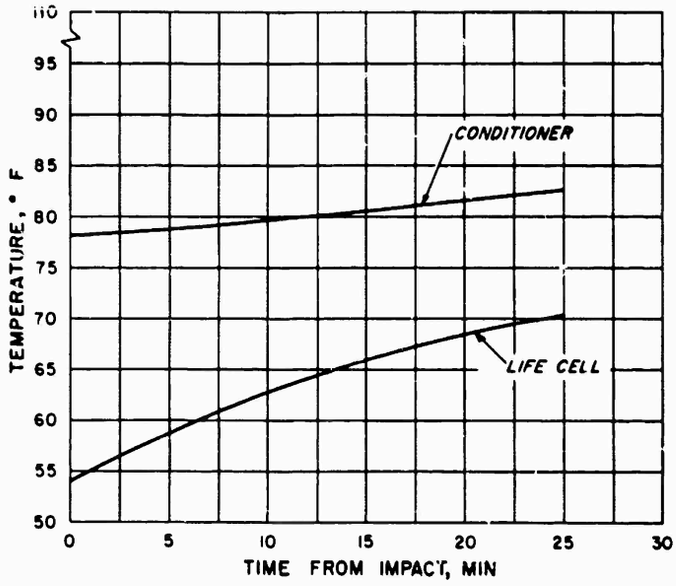

Figure 68. Life Cell and Conditioner Temperatures During Water Flotation

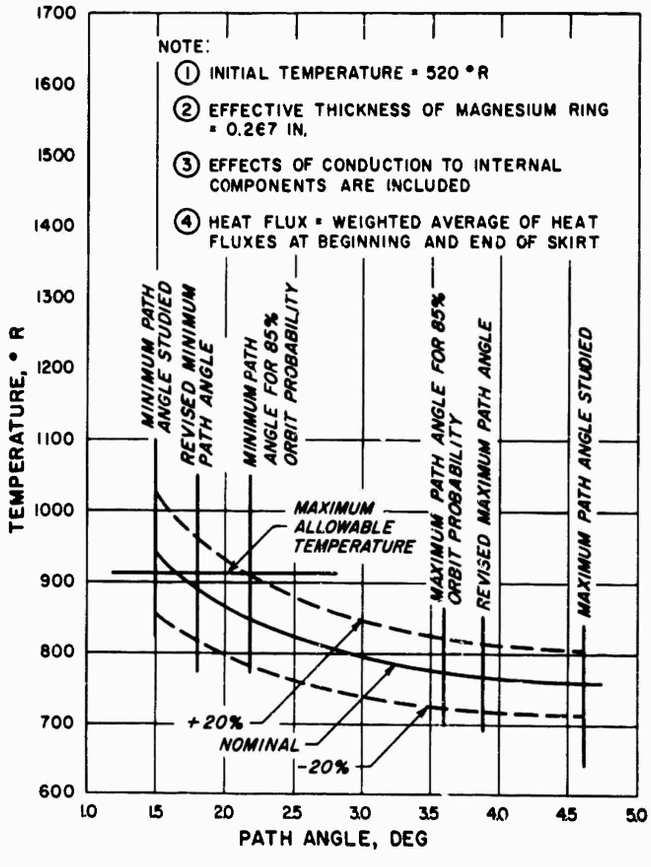

Figure 69. Average Magnesium Ring Temperature at Explosive Bolt During Parachute Ejection

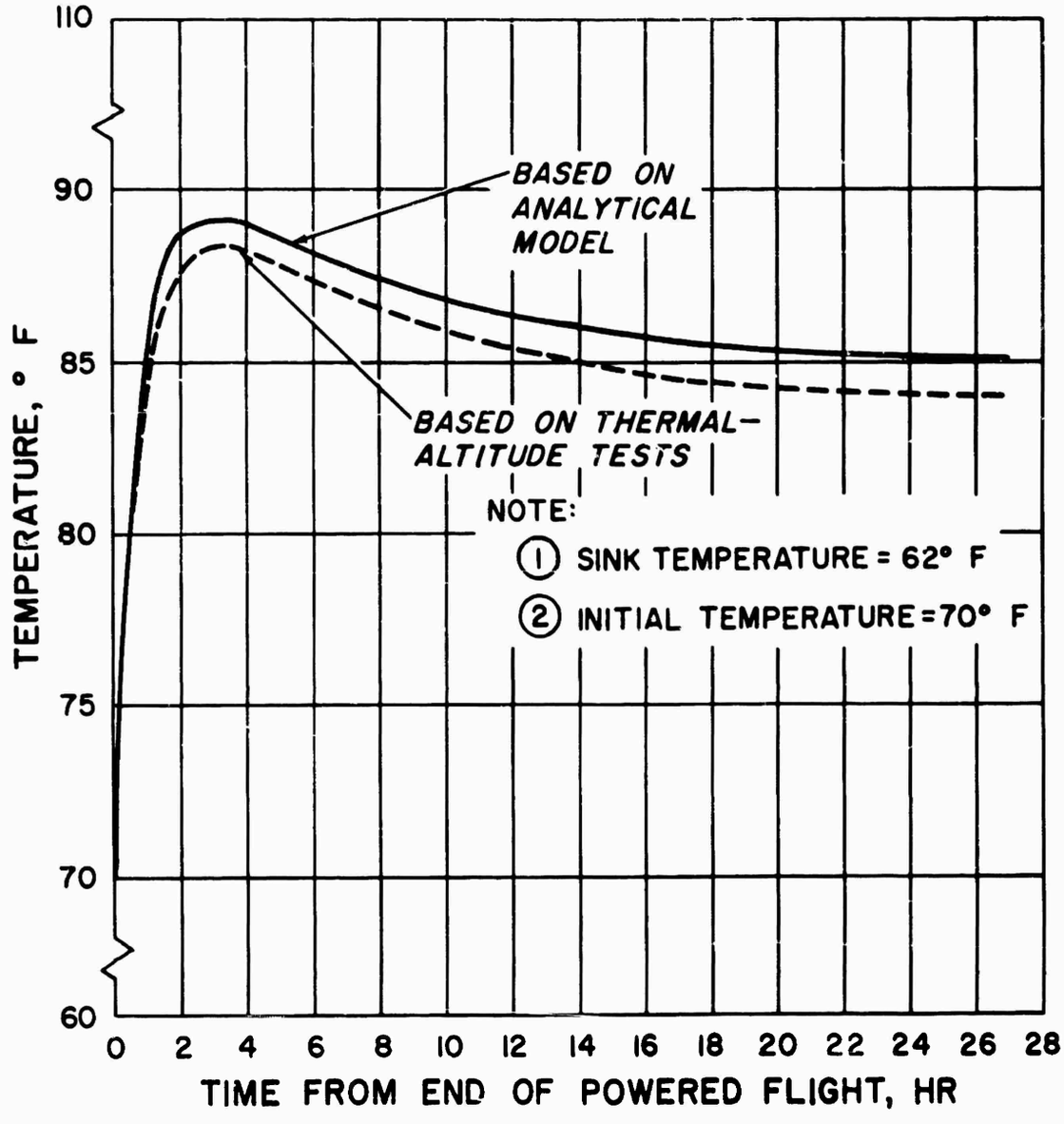

Figure 70. Life Cell Temperature During Powered Flight, Hottest Case

NATIONAL RECONNAISSANCE OFFICE
14675 Lee Road
Chantilly, VA 20151-1715

21 November 2012

Defense Technical Information Center
Attn: DTIC-OQ Information Security
8725 John J. Kingman Rd., Suite 0944
Ft. Belvoir, VA 22060-6218

To Whom It May Concern:

This concerns Technical Report AD-362544, ***Thermal Restudy of the Discoverer Mark 2 (Bio-Med) Vehicle***, by J. A. Segletes.

Subsequent to National Reconnaissance Office Mandatory Declassification Review request No. E13-0003, this record was approved for public release by the Acting Chief, Information Access and Release Team on 1 November 2012.

The attached declassified version of the document is now available for posting on the DTIC web site.

Please feel free to contact Ariela Berstein if you have any questions. She can be reached on 703 227-9411.

Sincerely,

Douglas J. Davis, Chief
Information Access and Release Team
Management Services and Operation
National Reconnaissance Office